This paper appears as:Carlos Eduardo Rodríguez-Pardo and Gaurav Sharma. Color control functions for multiprimary displays II: Variational robustness optimization. IEEE Trans. Image Proc., 29(1):1164--1176, 2020. DOI:10.1109/TIP.2019.2936992

Color Control Functions for Multiprimary Displays II: Variational Robustness Optimization

Carlos Eduardo Rodríguez-Pardo and Gaurav Sharma, *Fellow, IEEE*

***Abstract*—In a companion Part I paper, we presented a framework for analyzing robustness of color control functions (CCFs) for multiprimary displays against primary and observer variations and proposed a variational minimization for obtaining robust CCFs. The objective function proposed in the Part I paper combines two nonnegative terms that serve as useful figures of merit for quantitatively characterizing CCFs. The first term measures lack of smoothness of the CCFs and characterizes how well transitions in perceptual color space are preserved in the presence of the primary/observer variations. The second term measures deviation of the CCF, in the vicinity of the gray axis, from a specific axially linear CCF that provides perceptual invariance to the variations along the gray axis. In this paper, using calculus of variations, we develop an algorithm for numerically computing optimal CCFs under the proposed variational formulation. Using the proposed algorithm, we determine optimal CCFs for a several multiprimary display designs and assess and compare their performance against alternative approaches. The variationally optimal CCFs obtained using the proposed approach offer improvements over the alternatives, as assessed visually and via quantitative metrics measuring smoothness and invariance in the presence of primary variations. The relative improvements provided by the proposed CCF increase with increasing number of primaries.**

***Index Terms*—robust color control function, control values, device variation, observer variation, multiprimary displays, display color management, variational optimization.**

I. Introduction

Color management for a display typically uses a *color control function* (CCF) that assigns, to each color in the display's gamut, *control values* that are used to drive the display and reproduce the color. Multiprimary displays allow for alternative CCFs because control values for reproducing colors in the interior of the gamut are not uniquely determined. In a companion Part I paper [2], we presented a mathematical framework for analyzing the robustness of alternative CCFs for multiprimary display against variations in the displays primary spectral power distributions and the observers' color matching functions, variations that we refer to here as *primary variations*. In particular, we identified linearity and smoothness as key attributes of CCFs that determine the robustness of CCFs in the presence of primary variations. We showed that, thanks to the adaptation mechanisms in human color perception, a CCF that is linear in tristimulus values along the gray axis has the advantageous property that gray axis is perceptually invariant to primary variations. We also show that smoothness of the CCF helps preserve perceptual transitions in color. We incorporated both components of robustness, invariance along the gray axis and preservation of color transitions, into a single variational formulation for optimizing CCFs.

In this paper, we develop an algorithmic approach based on the calculus of variations for numerically computing optimal CCFs under the proposed variational formulation for robust CCFs. We present optimal robust CCFs computed using the proposed approach for several multiprimary designs and highlight the advantages of the proposed approach by comparing against alternative CCFs. Our approach is shown to offer smoother transitions in the interior of the display gamut when compared to other alternatives and to exhibit enhanced robustness in the presence of colorimetric variations in the primaries, with the relative advantage increasing with increasing number of primaries. The variational formulation and solution developed in the companion Part I paper [2] and the present paper, represent an entirely new approach to the of the problem of determining CCFs for multiprimary displays. In addition to the optimization methodology developed here, the variational formulation also offers new figures of merit for quantitatively characterizing different CCFs. In our assessments, the quantitative metric based on the figures of merit is found to correlate well with visual evaluation.

The manuscript is organized as follows: Section II provides a brief overview of the problem of determining a CCF for a multiprimary display; primarily with the objective of summarizing the notation and terminology from Part I. In Section III we present the variational formulation for optimizing CCFs for robustness against primary variations and introduce an iterative scheme for numerically computing optimal CCFs. An algorithmic statement and details for the numerical computation of the optimal CCFs are presented in Section IV. In Section V we summarize the settings used for the experiments and the evaluation metrics used for comparing alternative CCFs. Results for CCFs obtained using the proposed framework and comparisons with alternative CCFs for several multiprimary designs with $4, 5$ and 6 primaries are presented in VI. The trends observed in the results are discussed in Section VII. Section VIII concludes the main body of the paper with a summary of the main findings of this work. Appendices A–C provide details for various steps involved in the proposed

C.E. Rodríguez-Pardo is with the Department of Electrical and Computer Engineering, University of Rochester, Rochester, NY, 14627 USA (e-mail: c.rodriguezpardo@rochester.edu)

G. Sharma is with the Department of Electrical and Computer Engineering, Department of Computer Science, and Department of Biostatistics and Computational Biology, University of Rochester, Rochester, NY 14627, USA (e-mail: gaurav.sharma@rochester.edu)

The work presented here expands and advances the work that appeared as [1].

This paper has supplementary downloadable material available at http://ieeexplore.ieee.org, provided by the author. The material consists of a supplementary document.

approach.

II. Overview: CCFs for Multiprimary Displays

To provide relevant context, we briefly summarize the problem of determining CCFs for multiprimary displays from the Part I companion paper [2]. We rely on notation, terminology, and acronyms introduced in the Part I companion paper [2], which is coherent with the broader vector systems notation used in the signal processing community [3]–[5] for the discussion of color representation, processing, and color imaging systems.

Figure 1 illustrates the problem setting. A display system is characterized by its $(3 \times K)$ matrix of primaries $\mathbf{P} = [\mathbf{p}_1, \mathbf{p}_2, \ldots, \mathbf{p}_K]$, where $\mathbf{p}_k$ is the 3×1 vector of CIE XYZ tristimulus values for the k^{th} primary. Variations in the display primaries and observer color matching functions are modeled by setting $\mathbf{P} = \bar{\mathbf{P}} + \Delta\mathbf{P}$ where $\bar{\mathbf{P}}$ is the primary specification for the nominal display and $\Delta\mathbf{P}$ is the matrix of primary variations. The (tristimulus) gamut of the display $\mathcal{G} = \left\{\mathbf{t} | \mathbf{t} = \bar{\mathbf{P}}\boldsymbol{\nu}, \boldsymbol{\nu} \in [0,1]^K\right\}$ defines the range of (tristimulus) colors that the (nominal) display can reproduce. A color control function (CCF) $\boldsymbol{\alpha} : \mathcal{G} \rightarrow [0,1]^K$ for the display, determines, for each (in-gamut) tristimulus $\mathbf{t}_0$, a feasible control vector $\boldsymbol{\alpha}(\mathbf{t}_0)$ such that $\bar{\mathbf{P}}\boldsymbol{\alpha}(\mathbf{t}_0) = \mathbf{t}_0$. The *metameric control set* (MCS) $\Omega(\mathbf{t}_0)$ for an in-gamut tristimulus $\mathbf{t}_0$ is defined as the set of all feasible control vectors that reproduce the tristimulus $\mathbf{t}_0$ [6]. For $K \geq 4$, $\Omega(\mathbf{t}_0)$ contains an infinite number of feasible control values for a color $\mathbf{t}_0$ in the interior of the gamut and therefore an infinite number of alternative CCFs can be obtained.

The objective of the companion Part I paper [2] and this paper is to develop a framework and algorithm to determine optimal CCFs that are perceptually robust against the primary variations $\Delta\mathbf{P}$. Perceptual changes are best expressed in a perceptual color space, which we represent as a one-to-one nonlinear transformation $\mathscr{F}_{\mathbf{w}}(\cdot)$ of the tristimulus space, where $\mathbf{w}$ ($\bar{\mathbf{w}}$) denotes the *(nominal) display white* tristimulus, obtained when all control values are set to one. We denote by $\boldsymbol{\tau} = \mathscr{F}_{\mathbf{w}}(\mathbf{t})$ the perceptual color representation corresponding to a tristimulus $\mathbf{t}$ and by $\mathcal{G}_{\mathscr{F}}$ and $\boldsymbol{\alpha}^{\mathscr{F}}(\cdot)$ the gamut and the CCF representation, respectively, in the perceptual color space. We assume that perceptual color representation uses a standard three-dimensional lightness-chroma coordinate system $\boldsymbol{\tau} = [\tau_L, \tau_{c_1}, \tau_{c_2}]^T$, where τ_L represents the lightness and τ_{c_1} and τ_{c_2} represent the two opponent chroma coordinates, with $C_{\boldsymbol{\tau}} = \sqrt{\tau_{c_1}^2 + \tau_{c_2}^2}$ denoting the corresponding chroma. We denote by $\mathscr{C} = \{L, c_1, c_2\}$ the indices for perceptual color coordinates. For visualizing CCFs, we use the methodology introduced in [6] and summarized in the companion Part I paper [2]; the $K \times 1$ control vector $\boldsymbol{\alpha}(\mathbf{t}_0)$ is visualized using the corresponding $(K-3)$-dimensional control black space (CBS) component $\boldsymbol{\beta}(\mathbf{t}_0)$. Table I in the companion Part I paper [2] provides a list of symbols and acronyms that can also serve as a useful reference for readers of this paper. Additionally, to better convey intuition and to improve accessibility of the mathematical development, we highlight key points and findings by italicizing these.

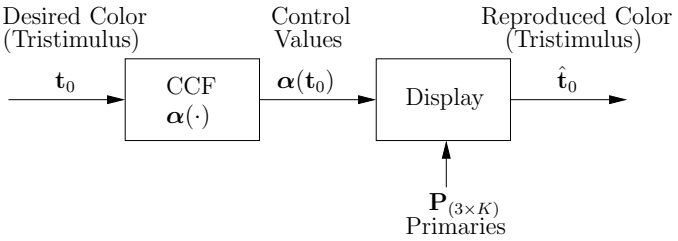

Fig. 1: Reproduction of a in-gamut color using a CCF $\boldsymbol{\alpha}(\cdot)$. To reproduce a desired color with tristimulus $\mathbf{t}_0 \in \mathcal{G}$, the display is driven with the control values $\boldsymbol{\alpha}(\mathbf{t}_0)$ and produces the tristimulus $\hat{\mathbf{t}}_0 = \mathbf{P}\boldsymbol{\alpha}(\mathbf{t}_0)$.

In the companion Part I paper [2], we analytically constructed a specific CCF, the axially linear CCF $\boldsymbol{\alpha}_{\mathcal{A}}^{\mathscr{F}}(\cdot)$ that has the *advantageous property that the gray axis is invariant to primary variations, but suffers from the limitation that its first order derivatives are discontinuous, which can be manifested as artifacts in renderings of smooth color trajectories*. Therefore, motivated by the objective of preserving color transitions, we formulated alternative metrics for optimization and evaluation of CCF robustness, whose definitions and optimization are the focus of the next section.

III. Variational Optimization for Computing Robust CCFs

In the companion Part I paper [2], we motivated and formulated two alternative variational optimization formulations (Equations (25) and (27) in [2]) for determining CCFs robust to primary variations. The second of these, allows representation of both formulations in a common framework as

$$\begin{aligned} &\min\ \Gamma(\boldsymbol{\alpha}^{\mathscr{F}}), \\ &\text{s.t. } \boldsymbol{\alpha}^{\mathscr{F}}(\boldsymbol{\tau}) \in \Omega(\mathbf{t}),\ \text{for all } \boldsymbol{\tau} \in \mathcal{G}_{\mathscr{F}}, \end{aligned} \tag{1}$$

where $\mathbf{t} = \mathscr{F}_{\bar{\mathbf{w}}}^{-1}(\boldsymbol{\tau})$ and the objective function

$$\Gamma(\boldsymbol{\alpha}^{\mathscr{F}}) = \int_{\mathcal{G}_{\mathscr{F}}} \mathcal{M}(\boldsymbol{\tau}, \boldsymbol{\alpha}^{\mathscr{F}}) d\boldsymbol{\tau}, \tag{2}$$

with

$$\mathcal{M}\big(\boldsymbol{\tau}, \boldsymbol{\alpha}^{\mathscr{F}}\big) = \mathcal{M}_{\Theta}\big(\boldsymbol{\tau}, \boldsymbol{\alpha}^{\mathscr{F}}\big) + \gamma I(\boldsymbol{\tau}, \sigma) \left\| \boldsymbol{\alpha}^{\mathscr{F}}(\boldsymbol{\tau}) - \boldsymbol{\alpha}_{\mathcal{A}}^{\mathscr{F}}(\boldsymbol{\tau}) \right\|^2, \tag{3}$$

$$\mathcal{M}_{\Theta}\big(\boldsymbol{\tau}, \boldsymbol{\alpha}^{\mathscr{F}}\big) = \sum_{k=1}^{K} \left\| \nabla \alpha_k^{\mathscr{F}}(\boldsymbol{\tau}) \right\|^2, \tag{4}$$

integrates two desirable attributes for a CCF $\boldsymbol{\alpha}^{\mathscr{F}}(\cdot)$ that improve robustness against primary variations: smoothness and linearity along the gray axis[1]*. Smoothness is encouraged by penalizing CCFs with high-valued derivatives as indicated by $\mathcal{M}_{\Theta}\big(\boldsymbol{\tau}, \boldsymbol{\alpha}^{\mathscr{F}}\big)$. Linearity along the gray axis is promoted by penalizing the deviation of $\boldsymbol{\alpha}^{\mathscr{F}}(\cdot)$ from the axially linear CCF $\boldsymbol{\alpha}_{\mathcal{A}}^{\mathscr{F}}(\cdot)$ around the gray axis, weighted according to the function $\gamma I(\boldsymbol{\tau}, \sigma)$, where the parameter γ determines the*

[1]Note that $\mathcal{M}(\cdot)$ and $\Gamma(\cdot)$ also depend on the first order derivatives of the CCF $\nabla\alpha_1^{\mathscr{F}}, \ldots, \nabla\alpha_K^{\mathscr{F}}$. We leave this dependency implicit for notational simplicity.

weighting of the penalty term along the gray axis, and $I(\boldsymbol{\tau}, \sigma)$ is a continuous and differentiable function chosen to localize the penalty in deviation from the CCF $\boldsymbol{\alpha}_{\mathcal{A}}^{\mathscr{F}}(\cdot)$ to an appropriate local vicinity of the gray axis. Optimizing the two attributes of smoothness and linearity along the gray axis leads to CCFs that offer perceptually invariant renderings of the gray axis and preserve color transitions in renderings in the presence of display primary variations.

Based on the calculus of variations [7], we propose an iterative projected gradient descent algorithm for numerically computing the optimal CCF in (1), which exploits the convexity of the MCS $\Omega(\mathbf{t})$ [6]. Starting from an initial CCF $\boldsymbol{\alpha}_0^{\mathscr{F}}(\cdot)$, the projected gradient descent algorithm [8], [9] computes successive CCF iterates as

$$\boldsymbol{\alpha}_{n+1}^{\mathscr{F}}(\boldsymbol{\tau}) = \mathcal{P}_{\Omega(\mathbf{t})}\big(\boldsymbol{\alpha}_n^{\mathscr{F}}(\boldsymbol{\tau}) - \eta \nabla_{\boldsymbol{\alpha}^{\mathscr{F}}} \Gamma(\boldsymbol{\alpha}_n^{\mathscr{F}}(\boldsymbol{\tau}))\big) \tag{5}$$

where n is the iteration number,

$$\mathcal{P}_A(\boldsymbol{\alpha}) = \underset{\boldsymbol{\omega} \in A}{\arg\min} \, \|\boldsymbol{\omega} - \boldsymbol{\alpha}\| \tag{6}$$

represents the projection of a vector $\boldsymbol{\alpha}$ onto the set A, η is the step size of the descent, and $\nabla_{\boldsymbol{\alpha}^{\mathscr{F}}}\Gamma$ is a $K \times 1$ vector whose k^{th} component corresponds to $\delta\Gamma/\delta\alpha_k^{\mathscr{F}}$, the variational derivative of Γ with respect $\alpha_k^{\mathscr{F}}(\boldsymbol{\tau})$, which is defined as [7]

$$\begin{aligned}\frac{\delta\Gamma}{\delta\alpha_k^{\mathscr{F}}} = &\frac{\partial}{\partial\alpha_k^{\mathscr{F}}}\left(\mathcal{M}(\boldsymbol{\tau}, \boldsymbol{\alpha}^{\mathscr{F}})\right) \\ &- \sum_{j \in \mathscr{C}} \frac{\partial}{\partial\tau_j} \frac{\partial}{\partial\alpha_{k,\tau_j}^{\mathscr{F}\prime}}\left(\mathcal{M}(\boldsymbol{\tau}, \boldsymbol{\alpha}^{\mathscr{F}})\right),\end{aligned} \tag{7}$$

where $\alpha_{k,\tau_j}^{\mathscr{F}\prime} = \partial\alpha_k^{\mathscr{F}}(\boldsymbol{\tau})/\partial\tau_j$, and $\delta\Gamma/\delta\alpha_k^{\mathscr{F}} = 0$ is the k^{th} Euler-Lagrange equation for the functional $\Gamma(\boldsymbol{\alpha}^{\mathscr{F}})$. In Appendix A we show that (7) can be expressed as

$$\frac{\delta\Gamma}{\delta\alpha_k^{\mathscr{F}}} = 2\gamma I(\boldsymbol{\tau}, \sigma)\left(\alpha_k^{\mathscr{F}}(\boldsymbol{\tau}) - \alpha_{\mathcal{A},k}^{\mathscr{F}}(\boldsymbol{\tau})\right) - 2\nabla^2\alpha_k^{\mathscr{F}}(\boldsymbol{\tau}). \tag{8}$$

where $\nabla^2\alpha_k^{\mathscr{F}}(\boldsymbol{\tau}) = \sum_{j\in\mathscr{C}} \partial^2\alpha_k^{\mathscr{F}}(\boldsymbol{\tau})/\partial\tau_j^2$ is the Laplacian of $\alpha_k^{\mathscr{F}}(\boldsymbol{\tau})$.

Note that for each $\boldsymbol{\tau} \in \mathcal{G}_{\mathscr{F}}$, the feasibility constraint on the control values in (1) is the convex MCS set $\Omega(\mathbf{t})$, and, for reasonable choices of γ and $I(\cdot)$, the functional $\Gamma(\boldsymbol{\alpha}^{\mathscr{F}})$ is strictly convex, as shown in Appendix A. In this strictly convex setting, the functional $\Gamma(\boldsymbol{\alpha}^{\mathscr{F}})$ has only one local minimum coincident with its global minimum, and the projected gradient descent algorithm converges to the globally optimal solution [9], [10].

We refer to the CCF $\boldsymbol{\alpha}_\Gamma^{\mathscr{F}}(\cdot)$ that optimizes $\Gamma(\boldsymbol{\alpha}^{\mathscr{F}})$ as the *optimal transition preserving CCF with gray axis invariance*. We note that when $\gamma = 0$, the only the first term corresponding to the attribute of smoothness of the CCF is optimized, and the objective function $\Gamma(\boldsymbol{\alpha}^{\mathscr{F}})$ coincides with the alternative function

$$\Theta(\boldsymbol{\alpha}^{\mathscr{F}}) = \int_{\mathcal{G}_{\mathscr{F}}} \mathcal{M}_\Theta\big(\boldsymbol{\tau}, \boldsymbol{\alpha}^{\mathscr{F}}\big)\, d\boldsymbol{\tau}, \tag{9}$$

defined in the Part I companion paper [2]. We refer to the CCF $\boldsymbol{\alpha}_\Theta^{\mathscr{F}}(\cdot)$ that minimizes $\Theta(\boldsymbol{\alpha}^{\mathscr{F}})$ as the *optimal transition preserving CCF*.

IV. Numerical Computation of CCF $\boldsymbol{\alpha}_\Gamma^{\mathscr{F}}(\cdot)$

The optimal CCF $\boldsymbol{\alpha}_\Gamma^{\mathscr{F}}(\cdot)$ is obtained numerically by solving the Euler-Lagrange equation in (5) via an iterative algorithm. For the numerical computations, the perceptual color space is discretized using a rectilinear 3-dimensional grid of points $\{\boldsymbol{\tau}_i\}_\epsilon$ that covers the display gamut $\mathcal{G}_{\mathscr{F}}$ with an internode spacing of ϵ perceptual units along each dimension. Via this discretization, the CCF $\boldsymbol{\alpha}_\Gamma^{\mathscr{F}}(\cdot)$ is represented as a three-dimensional look-up-table (LUT) and values at points between the LUT nodes are determined via trilinear interpolation [11, Chap. 5]. The overall procedure for numerical computation of $\boldsymbol{\alpha}_\Gamma^{\mathscr{F}}(\cdot)$ over the grid points is summarized in Algorithm 1. All functions and operators are computed for each node of the grid. In particular, the functional $\Gamma(\boldsymbol{\alpha}^{\mathscr{F}})$ is approximated by

$$\Gamma(\boldsymbol{\alpha}^{\mathscr{F}}) \approx \sum_{\boldsymbol{\tau} \in \{\boldsymbol{\tau}_i\}_\epsilon \cap \mathcal{G}_{\mathscr{F}}} \epsilon^3 \mathcal{M}(\boldsymbol{\tau}, \boldsymbol{\alpha}^{\mathscr{F}}), \tag{10}$$

which improves in accuracy with decreasing ϵ. For the discrete approximation of the variational derivative (8), the Laplacian is computed using the 27 point stencil approximation proposed in [12], which improves rotational symmetry over the standard 7 point stencil approximation, reducing directional dependence of the errors on the grid's rectilinear orientation. Required gradients of the functionals are computed using the 19 point stencil approximation from [12] that conforms with the chosen Laplacian approximation. Appendix C details both these numerical computations. The gradient projection step (Eqn. (5), equivalently, Step 10 in Algorithm 1) requires the projection of control vectors onto the MCS $\Omega(\mathbf{t})$, Appendix B outlines the computation of this projection via a recursive algorithm that relies on the fact that $\Omega(\mathbf{t})$ is a convex polytope.

Although $\{\boldsymbol{\tau}_i\}_\epsilon$ is a regular grid, the actual support for the CCF is defined by the gamut $\mathcal{G}_{\mathscr{F}}$, which is an irregular solid that can also have concave surfaces. This implies that LUT node values for points outside the gamut are considered when computing the Laplacian and the gradients for nodes adjacent to the surface of the gamut. Inaccuracies can be avoided by noting that control vectors for colors on the gamut surface are unique [13], thus, they represent boundary conditions for the optimization problem. Control values for LUT nodes that are outside the gamut but neighbors of in-gamut points are, therefore, set such that interpolation yields the correct CCF values on the gamut surface.

Most of the operations for the gradient descent scheme in Algorithm 1, including the computation of the Laplacian, can be reduced to additions and subtractions that can be efficiently implemented as filter operators in the three dimensional color space. The number of operations depends on the size of the grid, which in turn depends on the size of the gamut and the parameter ϵ. For each node, there are a total of $61 \times K$ operations for the gradient descent, disregarding the projection. The projection on the MCS, on the other hand, is an optimization problem in $\mathbb{R}^K$ whose complexity is heavily dependent on K and the chosen solution strategy. We note, however, that computational complexity is usually not of strong concern for this problem, because the computation of the CCF is typically performed off-line and only once for a given display design.

Algorithm 1: Computation of Optimal CCF $\boldsymbol{\alpha}_{\Gamma}^{\mathscr{F}}$

Input : $\{\boldsymbol{\tau}_i\}_\epsilon$: Rectangular grid covering $\mathcal{G}_{\mathscr{F}}$, with nodes $\boldsymbol{\tau}_i$ every ϵ perceptual units.
σ, γ: Weighting Function Parameters,
$\left\{\boldsymbol{\alpha}_0^{\mathscr{F}}(\boldsymbol{\tau}_i)\right\}_\epsilon$: Initial CCF (over grid)
$\left\{\boldsymbol{\alpha}_{\mathcal{A}}^{\mathscr{F}}(\boldsymbol{\tau}_i)\right\}_\epsilon$: Axially Linear CCF (over grid)
η: Gradient descent step-size
ρ : Convergence tolerance

Output: $\{\boldsymbol{\alpha}_\Gamma(\boldsymbol{\tau}_i)\}_\epsilon$: Optimal CCF for each node on grid.

$n \leftarrow 0$; // Initialize iteration counter
repeat
  forall $\boldsymbol{\tau} \in \{\boldsymbol{\tau}_i\}_\epsilon$ **do**
    /* Variational gradient of Γ at $\boldsymbol{\alpha}_n^{\mathscr{F}}(\boldsymbol{\tau}) = [\alpha_{n,1}^{\mathscr{F}}(\boldsymbol{\tau}), \ldots, \alpha_{n,K}^{\mathscr{F}}(\boldsymbol{\tau})]$ */
    for $k \leftarrow 1$ **to** K **do**
      $\delta\Gamma/\delta\alpha_{n,k}^{\mathscr{F}} \leftarrow -2\nabla^2\alpha_{n,k}^{\mathscr{F}}(\boldsymbol{\tau}) + 2\gamma I(\boldsymbol{\tau},\sigma)\left(\alpha_{n,k}^{\mathscr{F}}(\boldsymbol{\tau}) - \alpha_{\mathcal{A},k}^{\mathscr{F}}(\boldsymbol{\tau})\right)$;
    end
    $\nabla_{\boldsymbol{\alpha}}\Gamma \leftarrow \left[\delta\Gamma/\delta\alpha_{n,1}^{\mathscr{F}}, \ldots, \delta\Gamma/\delta\alpha_{n,K}^{\mathscr{F}}\right]^T$;
    if $\boldsymbol{\tau} \in \mathcal{G}_{\mathscr{F}}$ **then**
      // Projected Gradient Descent
      // See Algo. 2 for projection
      $\mathbf{t} \leftarrow \mathscr{F}^{-1}(\boldsymbol{\tau})$;
      $\boldsymbol{\alpha}_{n+1}^{\mathscr{F}}(\boldsymbol{\tau}) \leftarrow \mathcal{P}_{\Omega(\mathbf{t})}\left(\boldsymbol{\alpha}_n^{\mathscr{F}}(\boldsymbol{\tau}) - \eta\nabla_{\boldsymbol{\alpha}}\Gamma\right)$;
    end
  end
  $n \leftarrow (n+1)$;
until $\max_i \left\|\boldsymbol{\alpha}_n^{\mathscr{F}}(\boldsymbol{\tau}_i) - \boldsymbol{\alpha}_{n-1}^{\mathscr{F}}(\boldsymbol{\tau}_i)\right\| < \rho$;
$\boldsymbol{\alpha}_\Gamma^{\mathscr{F}} \leftarrow \boldsymbol{\alpha}_n^{\mathscr{F}}$; /* Assign output */

The optimal transition preserving CCF $\boldsymbol{\alpha}_\Theta^{\mathscr{F}}(\cdot)$ that minimizes $\Theta(\boldsymbol{\alpha}^{\mathscr{F}})$ can also be computed numerically by using Algorithm 1 with $\gamma = 0$ (with the same discretized LUT representation).

V. Experimental Settings and Evaluation Methodology

Before presenting results of CCFs designed with the proposed methodology, we first summarize the experimental settings and the evaluation methodology. First, we define the primary systems we use in our experiments. Then, we describe the alternative CCFs used in the comparisons and define the metrics and the visualization approach we use for comparisons. Finally, we specify the algorithmic parameters used in Algorithm 1 for obtaining the CCFs with the proposed framework.

A. Primary Systems for Evaluation

To validate proposed strategy we compute the optimal CCF for a set of primary configurations with different characteristics. We consider systems with $K = 4, 5$ and 6 primaries, which are obtained from a variety of primary design strategies, and whose CIE $x - y$ chromaticity gamuts are presented in Fig. 2. The tristimulus values corresponding to the primaries are tabulated in Section S.III of the Supplementary material accompanying this paper.

In particular, we denote by $\mathbf{P}_R^{(4)}$ the primary matrix for the four-primary display design proposed in [14], where the relative luminance of the primaries were chosen to maximize the display white luminance. The primary matrices for the display systems with four and five primaries $\mathbf{P}_M^{(4)}$ and $\mathbf{P}_M^{(5)}$, respectively, are obtained from the multi-objective optimization strategy described in [15] that optimizes chromaticity gamut coverage and observer metamerism[2]. Finally, the primary matrices $\mathbf{P}_U^{(4)}$, $\mathbf{P}_U^{(5)}$ and $\mathbf{P}_U^{(6)}$ are obtained from [16] as the primary configurations with $K = 4, 5$ and 6, primaries respectively, optimized with the design objective of having the maximum luminance for each in-gamut chromaticity in uniform proportion to the luminance of the optimal surface color of the same chromaticity [17]. The primary systems enumerated here are useful examples, we note, however, that our proposed methodology is general and appicable for arbitrary multiprimary designs. To emphasize this aspect, in Section S.VI of the Supplementary Materials we define and present results for two additional primary systems that are of potential interest in practice.

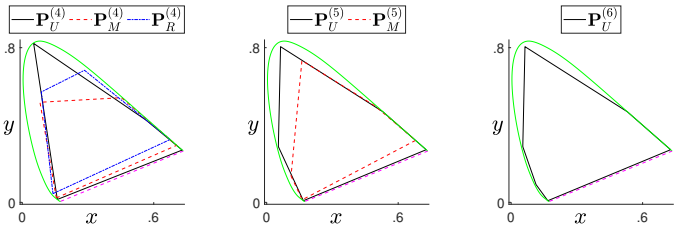

Fig. 2: CIE $x - y$ chromaticity gamut of the multiprimary displays used for the evaluation of the proposed CCF, with (a) $K = 4$, (b) $K = 5$, and (c) $K = 6$ primaries.

B. Benchmarked CCFs

We compare the optimal transition-preserving CCF $\boldsymbol{\alpha}_\Gamma(\cdot)$ and the axially linear CCF $\boldsymbol{\alpha}_{\mathcal{A}}(\cdot)$, with CCFs obtained from alternative strategies.

Besides the random CCF $\boldsymbol{\alpha}_\sim(\cdot)$, we include in our analysis $\boldsymbol{\alpha}_\mu(\cdot)$, the CCF defined for each color $\mathbf{t}$ as the center of mass of the MCS $\Omega(\mathbf{t})$, a strategy proposed in [18] for a six primary display. For $K = 4$, this strategy matches the average of the vertices of the $\Omega(\mathbf{t})$, a strategy proposed in [6].

We also consider $\boldsymbol{\alpha}_{p-}(\cdot)$, the CCF that yields minimal optical power usage[3], when used on emissive displays, like OLEDs. This strategy was initially proposed in [19] and characterized in [6], [20]. In particular, the minimal power

[2]These primary designs cover 65% of the CIE $u'v'$ chromaticity space and correspond to the Pareto-optimal configurations for chromaticity gamut coverage and observer metamerism, with the multi-observer tristimulus approximation (MOTA) strategy used for computation of control values.

[3]Optical power cannot be uniquely estimated using only the specification of the primary tristimuli. We model the spectral distribution of the primaries as Gaussian functions constrained to match the corresponding primary tristimuli, which allows ready computation of the optical power [6].

can be expressed as a linear programing optimization problem over the MCS, hence, optimal control value corresponds to one of the vertices of the MCS. For reference, we also include $\boldsymbol{\alpha}_{p+}(\cdot)$, the CCF that maximizes optical power [6], and at each color corresponds to another vertex of the MCS.

C. Evaluation: Metrics and Visualization

To evaluate and compare CCFs computed using the proposed approach against alternatives, we use a set of metrics that quantify the desired attributes of CCF smoothness and invariance along the gray axis.

As a *global (i.e., average over the entire gamut $\mathcal{G}_{\mathscr{F}}$) metric of relative lack of smoothness of a CCF*, we use

$$\Theta^* \stackrel{\text{def}}{=} \frac{\Theta(\boldsymbol{\alpha}^{\mathscr{F}}) - \Theta(\boldsymbol{\alpha}_{\Theta}^{\mathscr{F}})}{\Theta(\boldsymbol{\alpha}_{\Theta}^{\mathscr{F}})}. \tag{11}$$

Since $\boldsymbol{\alpha}_{\Theta}^{\mathscr{F}}(\cdot)$ minimizes Θ, the Θ^* metric is nonnegative for all CCFs and smaller values indicate smoother (better) CCFs. For many of the CCFs, the lack of smoothness is localized in specific regions of the gamut. For instance, in the companion Part I paper [2], we showed that the axially linear CCF $\boldsymbol{\alpha}_{\mathcal{A}}^{\mathscr{F}}(\cdot)$ is continuous with continuous derivatives (hence smooth) in the interior of quadrangle pyramids partitioning the gamut but has discontinuities in the Jacobian (and therefore directional derivatives) at the intersections of adjacent quadrangle pyramids. Therefore, *judgments of smoothness are more appropriately made locally*, so we use (see (4))

$$\mathcal{M}_{\Theta}^*(\boldsymbol{\tau}) \stackrel{\text{def}}{=} \frac{\mathcal{M}_{\Theta}(\boldsymbol{\tau}, \boldsymbol{\alpha}^{\mathscr{F}}) - \mathcal{M}_{\Theta}(\boldsymbol{\tau}, \boldsymbol{\alpha}_{\Theta}^{\mathscr{F}})}{\mathcal{M}_{\Theta}(\boldsymbol{\tau}, \boldsymbol{\alpha}_{\Theta}^{\mathscr{F}})} \tag{12}$$

as a *local metric of relative lack smoothness of a CCF*.

A perceptual assessment of the impact of primary variations is obtained by computing the difference between the display renderings of a color $\boldsymbol{\tau}$, produced by the nominal display primaries, and $\hat{\boldsymbol{\tau}}$, produced when variations are introduced in the primaries. To consider the differences in the conditions of adaptation of both scenarios, we obtain this assessment by computing the Euclidean distance between $\boldsymbol{\tau}$ and $\hat{\boldsymbol{\tau}}' = \mathscr{F}_{\bar{\mathbf{w}}}\left(\mathbf{C}_{\mathbf{w}}^{\bar{\mathbf{w}}}\mathbf{P}\boldsymbol{\alpha}^{\mathscr{F}}(\boldsymbol{\tau})\right)$, the perceptual representation for $\hat{\boldsymbol{\tau}}$ when considering changes in the visual system's adaptation from the display to the nominal white, which is modeled via the 3×3 chromatic adaptation transform $\mathbf{C}_{\mathbf{w}}^{\bar{\mathbf{w}}} \stackrel{\text{def}}{=} \boldsymbol{\Psi}^{-1}\mathbf{D}_{(\boldsymbol{\Psi}_{\bar{\mathbf{w}}})}\mathbf{D}_{(\boldsymbol{\Psi}_{\mathbf{w}})}^{-1}\boldsymbol{\Psi}$ in tristimulus space, where $\mathbf{D}_{\mathbf{a}}$ denotes a square diagonal matrix with the vector $\mathbf{a}$ as its diagonal and $\boldsymbol{\Psi}$ is transformation from the tristimulus space to the cone response space

Thus, we follow the steps shown in Fig. 3 to compute the perceptual difference

$$\Delta E\left(\boldsymbol{\tau}, \hat{\boldsymbol{\tau}}'\right) = \sqrt{(\tau_L - \hat{\tau}'_L)^2 + (\tau_{c_1} - \hat{\tau}'_{c_1})^2 + (\tau_{c_2} - \hat{\tau}'_{c_2})^2}. \tag{13}$$

We compute $\Delta E(\cdot)$ for colors on the gray axis to assess the invariance provided by CCFs. Since such differences depends on the particular variation of the primaries, to obtain a better idea of the ability of the CCF to offer gray axis invariance, we perform a Monte Carlo experiment, where the tristimulus of the variations for each primary are randomly generated (on a sphere with radius equaling 10% of the norm of the primary).

As smoothness and invariance are better judged through localized evaluation, we provide visualizations for renderings of different color trajectories obtained by the CCFs on the display systems with primary variations. The visualizations are restricted to the sRGB gamut to allow viewers to see these on common displays. Figure 4 summarizes the visualization strategy.

D. Algorithm and Implementation Parameters

We use the Gaussian function $I(\boldsymbol{\tau}, \sigma) = e^{-\frac{1}{2}(C\boldsymbol{\tau}/\sigma)^2}$, as weighing function for the functional $\Gamma(\boldsymbol{\alpha}^{\mathscr{F}})$. We use Algorithm 1 to compute the CCF $\boldsymbol{\alpha}_{\Gamma}^{\mathscr{F}}(\cdot)$, with parameter settings $\gamma = 20, \sigma = 5$, on a rectangular grid of points $\{\boldsymbol{\tau}_i\}_{\epsilon}$, covering the entire display gamut $\mathcal{G}_{\mathscr{F}}$ with a regular spacing of $\epsilon = 2$ perceptual units, over the perceptually uniform space CIELUV [22]. We also make sure the grid includes samples along the gray axis, given its importance for color reproduction. In Algorithm 1, we use the axially linear CCF $\boldsymbol{\alpha}_{\mathcal{A}}^{\mathscr{F}}(\cdot)$ as initialization for the projected gradient scheme. We obtain the CCF $\boldsymbol{\alpha}_{\Theta}^{\mathscr{F}}(\cdot)$ by setting $\gamma = 0$ in Algorithm 1 and by setting the remaining parameters to the values described above. The computation of the global and local lack of smoothness metrics Θ^* and $\mathcal{M}_{\Theta}^*(\boldsymbol{\tau})$ is also performed on the same sampling grid used for the numerical evaluation of the CCF. The computations of $\Delta E(\cdot)$ color differences in (13) used 50 uniformly spaced samples on the L^* axis and 1000 Monte Carlo iterations.

VI. Results

We report results from the *quantitative evaluation of the CCFs obtained with the proposed methodology, as well as visual assessments of their performance when reproducing color trajectories on display systems with primary variations*. We compare them with the evaluations obtained for the alternative CCFs specified in Section V-B. Given the number of display systems evaluated here, we present visual results that highlight the key points, and defer additional results to the Supplementary material accompanying this paper.

A. Quantitative Metrics

Results for the quantitative evaluation of CCFs for the multiprimary display systems with four, five, and six primaries, are summarized, respectively, in Tables I, II, and III. The tables indicate for each CCF the global metric for relative smoothness Θ^*, the maximum local metric of smoothness $\mathcal{M}_{\Theta}^*$ over the display gamut, as well as the average and maximum values of the perceptual difference $\Delta E(\cdot)$ obtained from the Monte Carlo experiment designed to evaluate gray axis invariance. Corresponding color difference values computed using alternative color difference formulae are included in Section S.IV in the supplementary materials. For reference and comparisons across different displays, the tables also show for each primary configuration the perceptual gamut volume $\mathcal{V}_{\mathscr{F}} = \int_{\mathcal{G}_{\mathscr{F}}} d\boldsymbol{\tau}$ and the normalized functional $\Theta_{\mathcal{V}_{\mathscr{F}}}(\boldsymbol{\alpha}^{\mathscr{F}}) \stackrel{\text{def}}{=} \Theta(\boldsymbol{\alpha}^{\mathscr{F}})/\mathcal{V}_{\mathscr{F}}$.

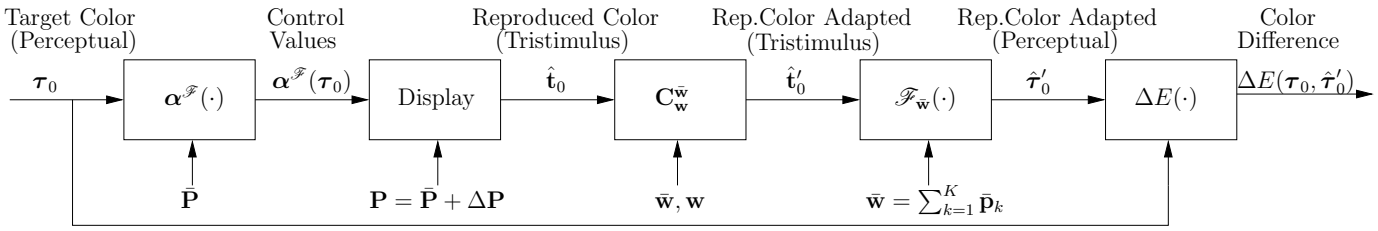

Fig. 3: Method used for evaluating perceptual color differences between the a target color $\boldsymbol{\tau}_0$ and the display reproduction $\hat{\boldsymbol{\tau}}_0$ using a CCF $\boldsymbol{\alpha}^{\mathscr{F}}(\cdot)$. For the target color $\boldsymbol{\tau}_0$, the CCF $\boldsymbol{\alpha}^{\mathscr{F}}(\cdot)$ provides the control values $\boldsymbol{\alpha}^{\mathscr{F}}(\boldsymbol{\tau}_0)$ that drive the display with primaries $\mathbf{P}$, producing a color with tristimulus $\hat{\mathbf{t}}_0$. For perceptual comparisons, the tristimulus $\mathbf{t}'_0 = \mathbf{C}_{\mathbf{w}}^{\bar{\mathbf{w}}}\hat{\mathbf{t}}_0$ expresses the chromatic adaptation of $\hat{\mathbf{t}}_0$ from the display white $\mathbf{w}$ to the nominal white $\bar{\mathbf{w}}$ and $\hat{\boldsymbol{\tau}}'_0$ is obtained as perceptual representation for the adapted tristimulus $\mathbf{t}'_0$. The Euclidean distance $\Delta E(\boldsymbol{\tau}_0, \boldsymbol{\tau}'_0) \stackrel{\text{def}}{=} \left\|\boldsymbol{\tau}_0 - \hat{\boldsymbol{\tau}}'_0\right\|$ represents the perceptual color difference between the target color $\boldsymbol{\tau}_0$ and the reproduced color $\hat{\boldsymbol{\tau}}'_0$.

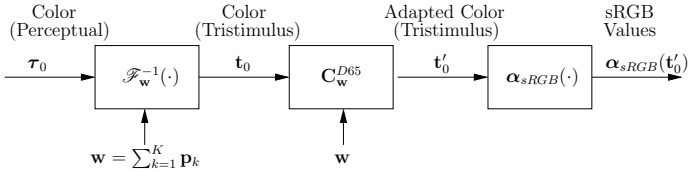

Fig. 4: Pipeline for visualizing colors produced by the multi-primary display with primaries $\mathbf{P}$ using a three primary display specified by the sRGB standard primaries [21]. A displayed color $\boldsymbol{\tau}_0$ is mapped to a corresponding tristimulus value $\mathbf{t}_0$ using the display white $\mathbf{w}$. The tristimulus $\mathbf{t}'_0 = \mathbf{C}_{\mathbf{w}}^{D65}\mathbf{t}_0$ expresses the chromatic adaptation of $\mathbf{t}_0$ from the display white $\mathbf{w}$ to the sRGB white, specified by illuminant D65. Chromatic adaptation is a process represented by the 3×3 matrix $\mathbf{D}_{\mathbf{w}}^{D65}$ that guarantees the right visualization of white. The sRGB values for $\mathbf{t}'_0$ are computed using the standard sRGB transformation, denoted by $\boldsymbol{\alpha}_{sRGB}(\cdot)$, which corresponds to the control value function for a sRGB display.

The tabulated results show that, among the evaluated CCFs, *the transition preserving CCF $\boldsymbol{\alpha}_{\Theta}^{\mathscr{F}}(\cdot)$ achieves the minimum values for the global smoothness metric Θ^* (as expected) and for the local smoothness metric $\mathcal{M}_{\Theta}^*$. The values of Θ^* for $\boldsymbol{\alpha}_{\Gamma}^{\mathscr{F}}(\cdot)$ are very small across the different display systems, indicating that overall the gamut, the CCFs obtained by the proposed methodology are similarly smooth. However, when examining the values of $\mathcal{M}_{\Theta}^*$ for $\boldsymbol{\alpha}_{\Gamma}^{\mathscr{F}}(\cdot)$, results show an evident loss in relative smoothness, although within 11% for the evaluated primary systems. The values of Θ^* for the axially linear CCF $\boldsymbol{\alpha}_{\mathcal{A}}^{\mathscr{F}}(\cdot)$ are the lowest after $\boldsymbol{\alpha}_{\Theta}^{\mathscr{F}}(\cdot)$ and $\boldsymbol{\alpha}_{\Gamma}^{\mathscr{F}}(\cdot)$, explained by the linearity of $\boldsymbol{\alpha}_{\mathcal{A}}^{\mathscr{F}}(\cdot)$ within the gamut-partitioning quadrangular pyramids described in the companion Part I paper [2]. The localized discontinuities of the first order derivatives of $\boldsymbol{\alpha}_{\mathcal{A}}^{\mathscr{F}}(\cdot)$ are reflected in the considerably higher values of $\mathcal{M}_{\Theta}^*$ showing that the maximum relative loss in smoothness is higher than 100% for the evaluated primary systems. Relative to $\boldsymbol{\alpha}_{\mathcal{A}}^{\mathscr{F}}(\cdot)$, both metrics for lack of smoothness are higher (worse) for the center of mass CCF $\boldsymbol{\alpha}_{\mu}^{\mathscr{F}}(\cdot)$ and for the optimal power CCFs $\boldsymbol{\alpha}_{p-}^{\mathscr{F}}(\cdot)$ and $\boldsymbol{\alpha}_{p+}^{\mathscr{F}}(\cdot)$, with the latter being pronouncedly worse.*

Results also show that the *relative smoothness advantage of $\boldsymbol{\alpha}_{\Theta}^{\mathscr{F}}$ over the other CCFs increases with the increasing number of primaries (K), as both Θ^* and $\mathcal{M}_{\Theta}^*$ increase for the other CCFs across the different primary designs*. This is particular evident when considering the results for the $\mathbf{P}_U^{(4)}$, $\mathbf{P}_U^{(5)}$, and $\mathbf{P}_U^{(6)}$, primary configurations that were obtained using the same primary-design methodology.

The statistics for the perceptual difference $\Delta E(\cdot)$ confirm that $\boldsymbol{\alpha}_{\mathcal{A}}^{\mathscr{F}}(\cdot)$ produces renderings of the gray axis that are invariant to primary variations, as both, average and mean $\Delta E(\cdot)$ are exactly zero. After $\boldsymbol{\alpha}_{\mathcal{A}}^{\mathscr{F}}(\cdot)$, the transition preserving CCFs $\boldsymbol{\alpha}_{\Gamma}^{\mathscr{F}}(\cdot)$ and $\boldsymbol{\alpha}_{\Theta}^{\mathscr{F}}(\cdot)$ offer the lowest perceptual color differences. However, while $\Delta E(\cdot)$ increases for $\boldsymbol{\alpha}_{\Theta}^{\mathscr{F}}(\cdot)$ with increasing numbers of primaries, it remains very close to zero for $\boldsymbol{\alpha}_{\Gamma}^{\mathscr{F}}(\cdot)$ for every primary system. This highlights that *the introduction of the gray axis invariance term in the formulation for $\boldsymbol{\alpha}_{\Gamma}^{\mathscr{F}}(\cdot)$ practically provides this CCF invariance along the gray axis at the cost of a rather minor decrease in smoothness*. The values of $\Delta E(\cdot)$ for $\boldsymbol{\alpha}_{\mu}^{\mathscr{F}}(\cdot)$ are higher, though similar, to the ones obtained by $\boldsymbol{\alpha}_{\Theta}^{\mathscr{F}}(\cdot)$. *The optimal power CCFs $\boldsymbol{\alpha}_{p-}^{\mathscr{F}}(\cdot)$ and $\boldsymbol{\alpha}_{p+}^{\mathscr{F}}(\cdot)$ have much larger errors and therefore lack the desirable property of gray axis invariance in the presence of primary variations*. Unlike the results for smoothness, the overall results for gray axis invariance seem to be insensitive to the number of primaries, except for $\boldsymbol{\alpha}_{\Theta}^{\mathscr{F}}(\cdot)$.

B. Visual Assessment Along Color Trajectories

Figure 5 shows the rendering of the gray axis of the five primary display system $\mathbf{P}_U^{(5)}$. Below the legend labels identifying the alternative CCFs considered, the first two plots at the top of Fig. 5 show for each CCF the corresponding CBS components β_1 and β_2 as function of the lightness τ_L. Below these plots, there are a series of stripes representing the display's renderings of the gray axis. The first one represents the rendering obtained by any CCF driving the display in the absence of primary variations, i.e., with the nominal primaries, while the remaining stripes show the results obtained when each of the evaluated CCFs is used to drive the display in the presence of primary variations. In this case, each primary underwent a variation equivalent to 5% of the primary's norm[4].

[4]The specific primaries used to generate the figures are tabulated in Table S.I in the Supplementary Material, where visualizations of color trajectories are also included for other primary systems.

	$\mathbf{P}_R^{(4)}$				$\mathbf{P}_U^{(4)}$				$\mathbf{P}_M^{(4)}$			
	Θ^*	$\mathcal{M}_\Theta^*$	ΔE		Θ^*	$\mathcal{M}_\Theta^*$	ΔE		Θ^*	$\mathcal{M}_\Theta^*$	ΔE	
CCF		max	av.	max		max	av.	max		max	av.	max
$\boldsymbol{\alpha}_\sim^{\mathscr{F}}$	0.8445	8.0353	0.78	8.19	1.0886	19.3772	0.79	8.41	0.7451	7.8825	1.02	12.19
$\boldsymbol{\alpha}_\Gamma^{\mathscr{F}}$	0.0002	0.3834	0.00	0.01	0.0002	0.4558	0.00	0.01	0.0003	0.2608	0.01	0.03
$\boldsymbol{\alpha}_\Theta^{\mathscr{F}}$	0.0000	0.0000	0.00	0.04	0.0000	0.0000	0.02	0.07	0.0000	0.0000	0.02	0.13
$\boldsymbol{\alpha}_\mathcal{A}^{\mathscr{F}}$	0.0438	2.7844	0.00	0.00	0.0710	10.2262	0.00	0.00	0.0261	3.7845	0.00	0.00
$\boldsymbol{\alpha}_\mu^{\mathscr{F}}$	0.1625	2.7747	0.37	2.58	0.2685	13.5641	0.57	3.69	0.1220	3.7679	0.74	5.43
$\boldsymbol{\alpha}_{p-}^{\mathscr{F}}$	0.3188	5.5702	1.59	10.44	0.3945	28.1628	1.46	8.78	0.2159	5.3102	1.85	12.64
$\boldsymbol{\alpha}_{p+}^{\mathscr{F}}$	0.4098	5.2443	2.06	13.56	0.4892	26.0728	2.22	13.52	0.3461	3.8031	2.85	19.54
$\Theta_{\mathcal{V}_\mathscr{F}}(\boldsymbol{\alpha}_\Theta^{\mathscr{F}})$		0.0278				0.0279				0.0272		
$\mathcal{V}_\mathscr{F}$		2243406				2569121				1847127		

TABLE I: Quantitative metrics for alternative CCFs for the $K = 4$ primary display systems. The CCFs obtained with the proposed variational approaches are identified (in this and subsequent tables) by yellow highlighting of the corresponding rows.

	$\mathbf{P}_U^{(5)}$				$\mathbf{P}_M^{(5)}$			
	Θ^*	$\mathcal{M}_\Theta^*$	ΔE		Θ^*	$\mathcal{M}_\Theta^*$	ΔE	
CCF		max	av.	max		max	av.	max
$\boldsymbol{\alpha}_\sim^{\mathscr{F}}$	0.3084	4.0686	2.32	20.10	0.2382	4.3696	2.73	23.50
$\boldsymbol{\alpha}_\Gamma^{\mathscr{F}}$	0.0001	0.1011	0.09	0.29	0.0001	0.0729	0.08	0.28
$\boldsymbol{\alpha}_\Theta^{\mathscr{F}}$	0.0000	0.0000	0.68	3.69	0.0000	0.0000	0.52	3.50
$\boldsymbol{\alpha}_\mathcal{A}^{\mathscr{F}}$	0.0760	3.5930	0.00	0.00	0.0580	4.1590	0.00	0.00
$\boldsymbol{\alpha}_\mu^{\mathscr{F}}$	0.1939	3.0005	1.06	7.20	0.1378	2.9818	0.87	5.76
$\boldsymbol{\alpha}_{p-}^{\mathscr{F}}$	0.4508	8.7881	2.00	12.63	0.3496	8.4079	3.77	24.26
$\boldsymbol{\alpha}_{p+}^{\mathscr{F}}$	0.5490	7.7572	3.57	22.53	0.5268	8.2090	4.19	27.32
$\Theta_{\mathcal{V}_\mathscr{F}}(\boldsymbol{\alpha}_\Theta^{\mathscr{F}})$		0.0319				0.0318		
$\mathcal{V}_\mathscr{F}$		2656404				2443413		

TABLE II: Quantitative metrics for alternative CCFs for the $K = 5$ primary display systems.

	$\mathbf{P}_U^{(6)}$			
	Θ^*	$\mathcal{M}_\Theta^*$	ΔE	
CCF		max	av.	max
$\boldsymbol{\alpha}_\sim^{\mathscr{F}}$	0.3434	3.5626	2.07	15.96
$\boldsymbol{\alpha}_\Gamma^{\mathscr{F}}$	0.0012	0.0741	0.09	0.29
$\boldsymbol{\alpha}_\Theta^{\mathscr{F}}$	0.0000	0.0000	0.97	5.41
$\boldsymbol{\alpha}_\mathcal{A}^{\mathscr{F}}$	0.1035	3.6316	0.00	0.00
$\boldsymbol{\alpha}_\mu^{\mathscr{F}}$	0.2062	3.0361	1.02	6.07
$\boldsymbol{\alpha}_{p-}^{\mathscr{F}}$	0.5819	7.6178	3.02	19.48
$\boldsymbol{\alpha}_{p+}^{\mathscr{F}}$	0.7306	8.7871	3.54	20.47
$\Theta_{\mathcal{V}_\mathscr{F}}(\boldsymbol{\alpha}_\Theta^{\mathscr{F}})$		0.0365		
$\mathcal{V}_\mathscr{F}$		2477917		

TABLE III: Quantitative metrics for alternative CCFs for the $K = 6$ primary display systems.

The graph below the stripes shows, as a function of the lightness τ_L, the perceptual difference $\Delta E(\cdot)$ between the gray axis renderings with and without primary variations (from their nominal values). Finally, below this graph there are two plots in the $\tau_L - \tau_{c_1}$ and $\tau_L - \tau_{c_2}$ planes depicting the desired values on the gray axis (shown by the black line) and the renderings obtained with the alternative CCFs in the presence of the primary variations.

From Fig. 5, we see that *the CBS components of* $\boldsymbol{\alpha}_\Gamma^{\mathscr{F}}(\cdot)$ *along the gray axis match very closely the CBS components of* $\boldsymbol{\alpha}_\mathcal{A}^{\mathscr{F}}(\cdot)$. *Given the properties of (tristimulus) linearity of* $\boldsymbol{\alpha}_\mathcal{A}^{\mathscr{F}}(\cdot)$, *the renderings of the gray axis produced by* $\boldsymbol{\alpha}_\Gamma^{\mathscr{F}}(\cdot)$ *are practically perceptually invariant*. This can be appreciated when comparing the stripes illustrating the renderings offered by $\boldsymbol{\alpha}_\Gamma^{\mathscr{F}}(\cdot)$ for the nominal display and the display with primary variations. *The visual assessment agrees with the corresponding plot of perceptual difference* $\Delta E(\cdot)$, *which is practically zero for every value of lightness*. The transition preserving CCF $\boldsymbol{\alpha}_\Theta^{\mathscr{F}}(\cdot)$ has CBS components that are similar, but not identical, to CBS components of $\boldsymbol{\alpha}_\Gamma^{\mathscr{F}}(\cdot)$. Although small, the differences are enough to introduce, under the primary variations, a green hue in the renderings of the gray axis, especially for the darkest grays. This effect is more pronounced for the center of mass CCF $\boldsymbol{\alpha}_\mu^{\mathscr{F}}(\cdot)$, whose CBS components exhibit stronger changes along lightness, producing a gray axis with green hue for the darker grays, and red hue in the lighter ones. The CBS plots for the optimal power CCFs $\boldsymbol{\alpha}_{p-}^{\mathscr{F}}(\cdot)$ and $\boldsymbol{\alpha}_{p+}^{\mathscr{F}}(\cdot)$ exhibit rapid changes in opposite directions. The corresponding gray axis renderings with primary variations are ramps with clear green and red hues, respectively. As a consequence, the corresponding plots of the perceptual differences exhibit some of the highest values among the evaluated CCFs.

Figure 6 shows the renderings for the trajectory defined by the radial line in CIELUV at constant lightness, $\tau_L = 75$, and opposing CIELUV hues corresponding to $h_{\boldsymbol{\tau}} = 86°$ and $h_{\boldsymbol{\tau}} = 266°$ for the four primary system $\mathbf{P}_R^{(4)}$ and the five primary system $\mathbf{P}_M^{(5)}$. Since this trajectory corresponds to a line segment varying along chroma for two complementary hues, results in Fig. 6 are shown as functions of chroma $C_{\boldsymbol{\tau}}$. To distinguish between the two hues, we add a negative sign to the chroma values for the points with $h_{\boldsymbol{\tau}} = 266°$, leaving a positive sign for the points with $h_{\boldsymbol{\tau}} = 86°$. In the plots for the CBS visualization and perceptual error, we also indicate with a gray shadowed box the color regions that fall outside the sRGB gamut. For visual assessment, the stripes representing the renderings are obtained by uniformly scaling the chroma of the renderings to fit inside the sRGB gamut. As this operation is performed in a perceptually uniform space, relative comparisons between scaled colors are still perceptually meaningful.

From Fig. 6, it can be seen that *the CBS components of the transition preserving CCFs* $\boldsymbol{\alpha}_\Theta^{\mathscr{F}}(\cdot)$ *and* $\boldsymbol{\alpha}_\Gamma^{\mathscr{F}}(\cdot)$ *match each*

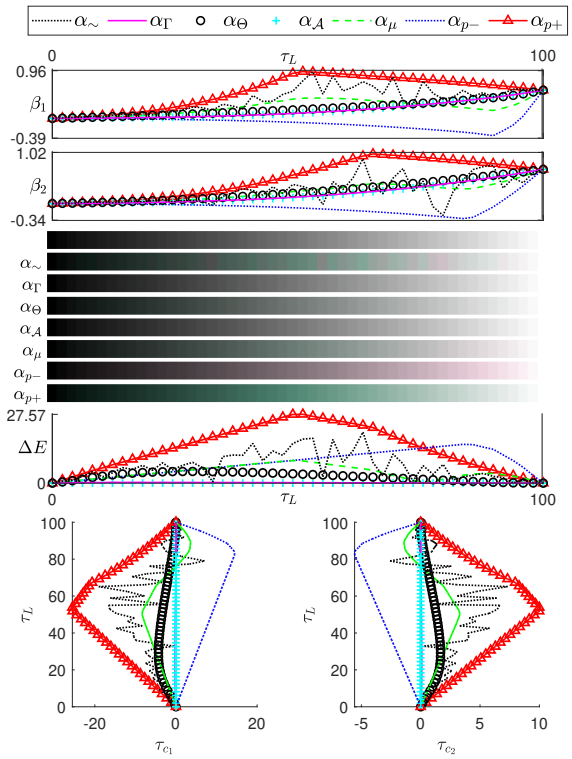

Fig. 5: Rendered gray axis for the five primary system $\mathbf{P}_U^{(5)}$. The CCFs are evaluated on 50 uniformly spaced samples along the ramp. From top to bottom: (1) legend labels identifying the alternative CCFs considered, (2) visualization of the CCFs in the CBS as function of lightness τ_L, (3) rendering of the gray ramp, (4) the perceptual color difference $\Delta E(\cdot)$ between the system with the nominal primary and the one with the primary variation, and (5) $\tau_L - \tau_{c_1}$-plane and $\tau_L - \tau_{c_2}$-plane plots depicting the desired ramp (in black) and the renderings obtained with the alternative CCFs in the presence of the primary variation. **To appreciate the color differences, please see the electronic version of the document.**

other along all the trajectory, for both primary configurations, as the requirement for gray axis invariance decays with chroma. In both cases, $\boldsymbol{\alpha}_\Theta^\mathscr{F}(\cdot)$ *and* $\boldsymbol{\alpha}_\Gamma^\mathscr{F}(\cdot)$ *are the smoothest functions among the evaluated CCFs, and so are the color transitions of the renderings produced by these CCFs. In contrast, for both systems, a discontinuity in the first order derivatives of* $\boldsymbol{\alpha}_\mathcal{A}^\mathscr{F}(\cdot)$ *appears at a color with high chroma* $C_{\boldsymbol{\tau}}$ *and* $h_{\boldsymbol{\tau}} = 86°$. Around that point, color artifacts emerge in the renditions produced by $\boldsymbol{\alpha}_\mathcal{A}^\mathscr{F}(\cdot)$ on the displays with primary variations. The artifacts are more pronounced for $\mathbf{P}_M^{(5)}$, as consequence of a strong change in the β_2 component of $\boldsymbol{\alpha}_\mathcal{A}^\mathscr{F}(\cdot)$, as shown in Fig. 6(b). While $\boldsymbol{\alpha}_\mu^\mathscr{F}(\cdot)$ is smooth along center of the trajectory, $\boldsymbol{\alpha}_\mu^\mathscr{F}(\cdot)$ changes rapidly at both ends of the trajectory, which translates into perceptual artifacts. Following the same trend as the gray axis, *the optimal power CCFs have CBS components that grow rapidly at the two ends of the trajectory and produce renderings with the highest values of* $\Delta E(\cdot)$.

VII. Discussion

Among the evaluated CCFs, apart from the random CCF, the optimal optical power CCFs $\boldsymbol{\alpha}_{p-}(\cdot)$ and $\boldsymbol{\alpha}_{p+}(\cdot)$ showed the worst results in the quantitative evaluations of smoothness and gray axis invariance, for both global and local metrics, and also in the visual assessments along specific trajectories. Moreover, the differences between $\boldsymbol{\alpha}_{p-}(\cdot)$ and $\boldsymbol{\alpha}_{p+}(\cdot)$ were significant: the corresponding CBS plots along specific trajectories changed in opposite directions and the visual examples exhibited distinct variations in the presence of primary variations. These results can be understood by recalling that the control values provided by $\boldsymbol{\alpha}_{p-}(\cdot)$ and $\boldsymbol{\alpha}_{p+}(\cdot)$ for each color are different vertices of the corresponding MCS. For $K = 4$ in particular, they are the two opposite endpoints of the MCS line segments. Hence, these CCFs define the bounding extremes when alternative CCFs are plotted along specific color trajectories in the CBS. When variations in the primaries occur, the differences in control values are expressed as perceptual differences in the color renderings, so $\boldsymbol{\alpha}_{p-}(\cdot)$ and $\boldsymbol{\alpha}_{p+}(\cdot)$ are the most sensitive to primary variations. This intuition extends to $K > 4$ primaries: the vertices for minimum and maximum power are usually distant from each other and the renderings of $\boldsymbol{\alpha}_{p-}(\cdot)$ and $\boldsymbol{\alpha}_{p+}(\cdot)$ exhibit significant pereceptual differences in the presence of primary variations.

In contrast, the CCF $\boldsymbol{\alpha}_\mu(\cdot)$, which is determined as the center of mass of MCS, offered better quantitative and visual results, when compared to the optimal power CCFs. However, $\boldsymbol{\alpha}_\mu(\cdot)$ also depends directly on the vertices of the MCS, which adversely affects both gray axis invariance and smoothness, as was shown in the results. Nevertheless, while Θ^* values for $\boldsymbol{\alpha}_\mu(\cdot)$ for every display system were higher than those of $\boldsymbol{\alpha}_\mathcal{A}(\cdot)$, the ratio between both quantities decreased with increasing number of primaries. A similar trend is found for $\mathcal{M}_\Theta^*$; for $K \geq 5$, the values of $\mathcal{M}_\Theta^*$ for $\boldsymbol{\alpha}_\mu(\cdot)$ were consistently better than those for $\boldsymbol{\alpha}_\mathcal{A}(\cdot)$. The dimensionality of the MCS for colors in the interior of the gamut increases with increasing number of primaries, going from one dimensional sets for $K = 4$, to three dimensional sets for $K = 6$. For many colors, this also increases the number of vertices for the MCSs, reducing the dependency that the center of mass has on individual vertices, explaining in part the improvement of $\boldsymbol{\alpha}_\mu(\cdot)$ relative to $\boldsymbol{\alpha}_\mathcal{A}(\cdot)$. *The dimensionality increase also increases the flexibility for choosing control values, which is exploited by the proposed methodology for optimization of CCFs and the metrics for smoothness improve for the proposed CCF* $\boldsymbol{\alpha}_\Theta(\cdot)$ *relative to those of alternative CCFs with increasing number of primaries* K.

Although, the proposed formulation is broadly applicable in any perceptual color space, for gridding the color space for numerical computation and for the illustrations, we have chosen the CIELUV color space. We outline briefly the reason for this choice over the more commonly used CIELAB space or alternative newer perceptual color spaces. As noted in the analysis in the Part I companion paper [2], the derivative discontinuities in the axially linear CCF are encountered at the intersection of quadrangle pyramids with a maximum

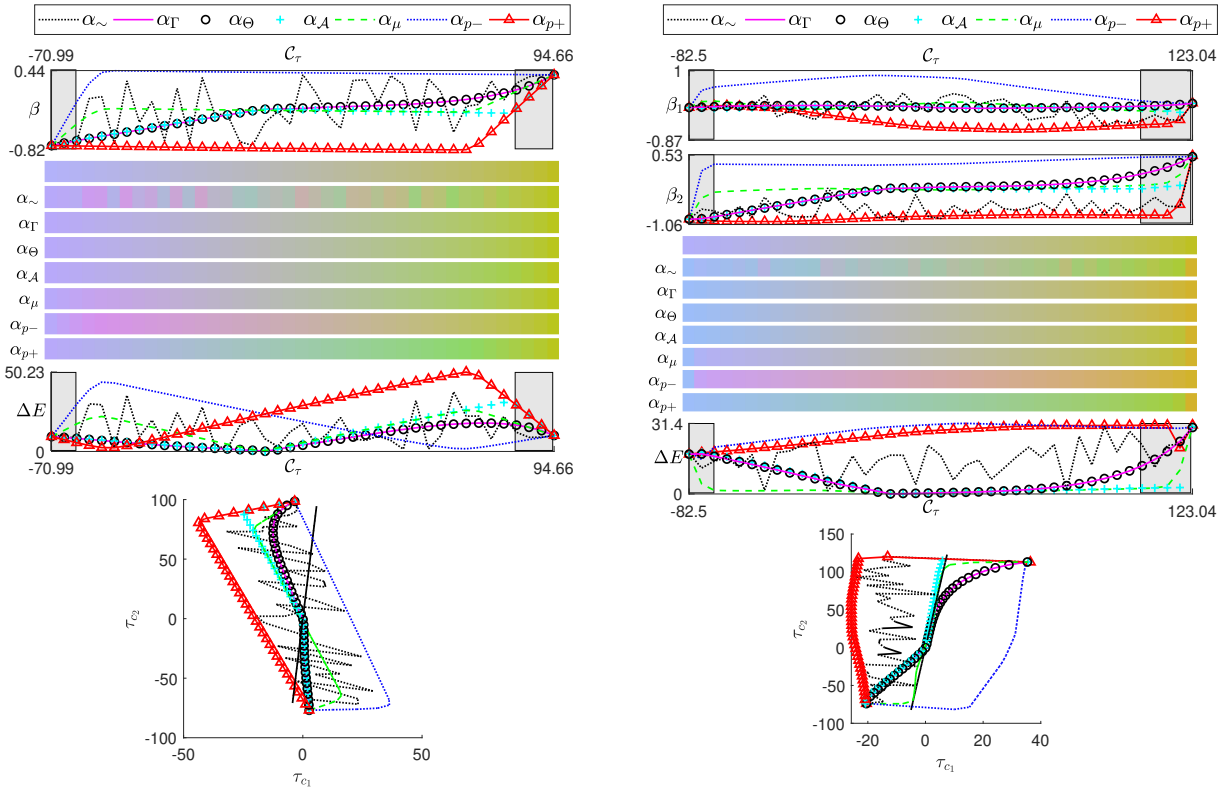

(a) (b)

Fig. 6: Radial line in CIELUV at constant lightness, $\tau_L = 75$, and opposing CIELUV hues corresponding to $h_{\boldsymbol{\tau}} = 86°$ and $h_{\boldsymbol{\tau}} = 266°$, for (a) the four primary system $\mathbf{P}_R^{(4)}$ and (b) the five primary system $\mathbf{P}_M^{(5)}$. The CCFs are evaluated on 40 uniformly spaced samples between the two extreme points on the gamut surface. For each of the subfigures (a) and (b), the following are presented, in order, from top to bottom: (1) legend labels identifying the alternative CCFs considered, (2) visualization of the CCFs in the CBS as function of chroma $C_{\boldsymbol{\tau}}$, (3) rendering of the ramp between the maximum chroma values for the two opposing hues $h_{\boldsymbol{\tau}} = 86°/266°$, (4) the perceptual color difference $\Delta E(\cdot)$ between the system with the nominal primary and the one with the primary variation, and (5) $\tau_{c_1} - \tau_{c_2}$-plane plot depicting the desired ramp (in black) and the renderings obtained with the alternative CCFs in the presence of the primary variation. For the purpose of illustration, chroma values along the two opposing hues $h_{\boldsymbol{\tau}} = 86°/266°$ are assigned positive and negative signs, respectively. The transparent gray boxes overlaid on the two ends identify the regions outside the sRGB gamut. **To appreciate the color differences, please see the electronic version of the document**.

magnitude of the discontinuity that occurs approximately in the lateral direction. The impact of these derivative discontinuities on color rendering is therefore best highlighted along radial hue lines of constant lightness that traverse the pyramidal boundaries in a lateral direction. To avoid the issues with the "hue nonlinearity" [23], [24] [11, pp. 33] and exaggeration of differences in the saturated blue region [25] for CIELAB, we use radial lines of constant lightness in CIELUV for the illustrations in Figs. 6, S.4, S.8, and S.9. We also preferred CIELUV over newer perceptual color spaces, such as CAM16 [26], because: (a) these newer spaces require additional parameters (minimally, assumptions on the surround and the absolute luminance for the test adapting field) that would add complexity to the presentation without changing the fundamental message and findings, and (b) the gray axis in these spaces exhibit slight numerical deviations from the CIELAB/CIELUV L^* axis, which would necessitate additional, not particularly insightful, explanation for the metrics reported for the axially linear CCF. For brevity and consistency with the gridding and the hue sampling space, the ΔE errors reported in Tables I– III have also been computed and reported in CIELUV. Corresponding errors computed using the CIELAB, CIEDE2000 [27], [28] and CAM16-UCS [26] color difference formulae are reported in Tables S.IV– S.VI in the Supplementary Materials. These exhibit identical trends to the results presented in Tables I– III and reinforce the findings already presented.

Variational approaches have been used in a variety of applications in image processing [29]–[31], including in color imaging [32]. The research effort represented in the companion Part I paper [2] and this paper, represents the first instance where the variational approach has been effectively introduced for the problem of determining CCFs for multiprimary displays. In contrast to most prior applications of variational approaches in image processing, where the color of an image is computed (a three dimensional function with rectangular

two dimensional support), the variational problem considered in this paper aims to optimize $K \geq 4$ dimensional functions whose support is the display gamut, a three dimensional and irregular solid.

Finally, we note that, in prior literature, the terms color control vectors and CCFs have not been formally defined; instead, a diverse set of alternative names have been used. For instance, color control vectors have been referred to as display drive levels [33], multiprimary color signal [34]–[36], control sequences [13], [20], [37], device control values [18], display signals [38], primary-color signals [19], or device control signals [39]. Similarly, the process for computing a CCF has been variously referred to as multiprimary color conversion method [19], [34], [38], [39] multiprimary control value decomposition [35]. multiprimary color decomposition [36], primary decomposition [40], or multiprimary color calibration functions [1]. We hope that the mathematical framework and terminology introduced in the companion Part I paper [2] and in this paper will also serve as a useful contribution to the community by providing formal structure with coherent nomenclature, which, if adopted, can help eliminate some of the confusion caused by the varied and inconsistent terms used previously.

VIII. Conclusion

This paper presented a methodology for computing color control functions (CCFs) for multiprimary color displays that are optimally robust against variations in display primaries. A numerical algorithm is developed based on the calculus of variations to optimize an objective function Γ that incorporates two desirable robustness attributes: perceptual invariance along the gray axis and preservation of color transitions. We present optimal CCFs obtained using the proposed methodology for a number of different multiprimary display designs and compare these against previously proposed alternative CCFs using both visual demonstrations and quantitative metrics. Results show that the optimized CCF $\boldsymbol{\alpha}^{\mathscr{F}}_{\Gamma}(\cdot)$, offers enhanced robustness to primary variation, when compared to alternative CCFs. The advantage of this CCF over the alternative strategies increases with the increment of the number of primaries.

Results also indicate that the proposed error metric Θ^* and its localized variant $\mathcal{M}^*_{\Theta}(\boldsymbol{\tau})$ can be used as figure of merit for the quantitative evaluation of smoothness, hence robustness, as evaluations of Θ^* ($\mathcal{M}^*_{\Theta}(\boldsymbol{\tau})$) for a variety of CCFs agree with visual assessments of renderings for displays with primary variations: the higher the Θ^* ($\mathcal{M}^*_{\Theta}(\boldsymbol{\tau})$), the greater the likelihood of renderings with artifacts and with higher perceptual differences with respect to renderings under nominal conditions. In particular, we observed that the axially linear CCF $\boldsymbol{\alpha}^{\mathscr{F}}_{\mathcal{A}}(\cdot)$, which consistently showed lower values for Θ^* across different primary configurations, showed problematic renderings only on trajectories crossing different pyramidal regions, and for colors further away from the gray axis, regions with high values of the localized metric $\mathcal{M}^*_{\Theta}(\boldsymbol{\tau})$.

On the other hand, strategies such as minimum optical power (applicable for emissive displays like OLEDs) result in control values on the vertices or edges of the MCS, exhibit particularly non-smooth behavior, resulting in higher values of the metric Θ^* ($\mathcal{M}^*_{\Theta}(\boldsymbol{\tau})$) and greater sensitivity to primary variations. This highlights the fact that exploiting flexibility of selecting the CCF in a multiprimary display to optimize other display attributes, e.g. power, may levy a penalty in terms of robustness to primary variations.

Appendix A
Variational Derivatives of $\Gamma(\boldsymbol{\alpha}^{\mathscr{F}})$

This appendix outlines the computation of variational derivatives in $\nabla_{\boldsymbol{\alpha}^{\mathscr{F}}}\Gamma(\boldsymbol{\alpha}^{\mathscr{F}})$ that are part of the gradient projection scheme for the numerical computation of the transition preserving CCFs (5). A comment on the convexity of $\Gamma(\boldsymbol{\alpha}^{\mathscr{F}})$ is also found ant the end this appendix.

The variational derivative of $\Gamma(\boldsymbol{\alpha}^{\mathscr{F}})$ with respect to the k^{th} component of $\boldsymbol{\alpha}^{\mathscr{F}}(\cdot)$, denoted by $\delta\Gamma/\delta\alpha^{\mathscr{F}}_k$, is defined as [7, p. 28]

$$\frac{\delta\Gamma(\boldsymbol{\alpha}^{\mathscr{F}})}{\delta\alpha^{\mathscr{F}}_k} = \frac{\partial}{\partial\alpha^{\mathscr{F}}_k}\mathcal{M}(\boldsymbol{\tau},\boldsymbol{\alpha}^{\mathscr{F}}) - \sum_{j\in\mathscr{C}}\frac{\partial}{\partial\tau_j}\frac{\partial}{\partial\alpha^{\mathscr{F}'}_{k,\mathcal{T}_j}}\mathcal{M}(\boldsymbol{\tau},\boldsymbol{\alpha}^{\mathscr{F}}). \tag{14}$$

The condition $\delta\Gamma/\delta\alpha^{\mathscr{F}}_k = 0$ then corresponds to the k^{th} Euler-Lagrange equation for the functional $\Gamma(\boldsymbol{\alpha}^{\mathscr{F}})$. To simplify presentation, in the rest of the appendix we drop the explicit dependency of Γ and $\mathcal{M}$ on the function $\boldsymbol{\alpha}^{\mathscr{F}}(\cdot)$ and $\boldsymbol{\tau}$.

By noting that the functional $\mathcal{M}$, defined in (3), can be expressed as

$$\mathcal{M} = \sum_{k=1}^{K}\sum_{j\in\mathscr{C}}\Big(\alpha^{\mathscr{F}'}_{k,\mathcal{T}_j}(\boldsymbol{\tau})\Big)^2 + \gamma I(\boldsymbol{\tau},\sigma)\sum_{k=1}^{K}\big(\alpha^{\mathscr{F}}_k(\boldsymbol{\tau}) - \alpha^{\mathscr{F}}_{\mathcal{A},k}(\boldsymbol{\tau})\big)^2, \tag{15}$$

we compute the first term on the right-hand-side of (14) as

$$\frac{\partial}{\partial\alpha^{\mathscr{F}}_k}\mathcal{M} = 2\gamma I(\boldsymbol{\tau},\sigma)\left(\alpha^{\mathscr{F}}_k(\boldsymbol{\tau}) - \alpha^{\mathscr{F}}_{\mathcal{A},k}(\boldsymbol{\tau})\right). \tag{16}$$

Similarly, for $j \in \mathscr{C}$

$$\frac{\partial}{\partial\alpha^{\mathscr{F}'}_{k,\mathcal{T}_j}}\mathcal{M} = 2\alpha^{\mathscr{F}'}_{k,\mathcal{T}_j}(\boldsymbol{\tau}), \tag{17}$$

which leads us to

$$\frac{\partial}{\partial\tau_j}\frac{\partial}{\partial\alpha^{\mathscr{F}'}_{k,\mathcal{T}_j}}\mathcal{M} = 2\frac{\partial^2}{\partial\tau_j^2}\alpha^{\mathscr{F}}_k(\boldsymbol{\tau}). \tag{18}$$

Next, using (16) and (18), the variational derivative in (14) can be expressed as

$$\frac{\delta\Gamma}{\delta\alpha^{\mathscr{F}}_k} = 2\gamma I(\boldsymbol{\tau},\sigma)\left(\alpha^{\mathscr{F}}_k(\boldsymbol{\tau}) - \alpha^{\mathscr{F}}_{\mathcal{A},k}(\boldsymbol{\tau})\right) - 2\nabla^2\alpha^{\mathscr{F}}_k(\boldsymbol{\tau}). \tag{19}$$

The convexity of the functional Γ can be confirmed by computing the Hessian matrix of $\mathcal{M}$ over every CCF component $\alpha^{\mathscr{F}}_k(\cdot)$, and the corresponding first order partial derivatives $\alpha^{\mathscr{F}'}_{k,\mathcal{T}_L}(\cdot), \alpha^{\mathscr{F}'}_{k,\mathcal{T}_{c1}}(\cdot), \alpha^{\mathscr{F}'}_{k,\mathcal{T}_{c2}}(\cdot)$, with $k = 1,\ldots,K$. From (16) and (17), the second order derivatives $\partial^2\mathcal{M}/\partial^2\alpha^{\mathscr{F}}_k = 2\gamma I(\boldsymbol{\tau},\sigma)$ and $\partial^2\mathcal{M}/\partial^2\alpha^{\mathscr{F}'}_{k,\mathcal{T}_j} = 2$ are positive[5] for all $\boldsymbol{\tau}$ in

[5]For reasonable choices of the indicator function the condition $I(\boldsymbol{\tau},\sigma) > 0$, and $\gamma > 0$.

the gamut, while the mixed derivatives are all zero. Therefore, the Hessian is a diagonal matrix with positive entries, thus the Hessian is positive definite, demonstrating the strict convexity of Γ [41].

APPENDIX B
PROJECTION ONTO THE MCS $\Omega(\mathbf{t})$

The MCS $\Omega(\mathbf{t})$ is a convex polytope contained in an affine subspace (i.e., a translate of a subspace) of the $(K-3)$ dimensional CBS. If the control vector is not already in the MCS $\Omega(\mathbf{t})$, its projection onto the MCS polytope lies on a facet of the polytope, which is itself a polytope contained in an affine subspace of the CBS with a dimensionality between $(K-4)$ and 0. This enables a recursive scheme for the computation of the projection of a vector $\boldsymbol{\alpha} \in \mathbb{R}^K$ onto the MCS $\Omega(\mathbf{t})$. To simplify notation, we consider the projection $\mathcal{P}_\Xi(\boldsymbol{\alpha})$ of a vector $\boldsymbol{\alpha} \in \mathbb{R}^K$ onto a general convex polytope $\Xi = \text{conv}\,(\boldsymbol{\nu}_1, \ldots, \boldsymbol{\nu}_{N_\Xi})$, where $\boldsymbol{\nu}_i \in \mathbb{R}^K$ is the i^{th} vertex of Ξ and N_Ξ is the total number of vertices. When $N_\Xi = 1$, the projection is trivially obtained as $\mathcal{P}_\Xi(\boldsymbol{\alpha}) = \boldsymbol{\nu}_1$. For $N_\Xi \geq 2$, let $S \subseteq \mathbb{R}^K$ be the affine subspace of minimal dimensionality that contains Ξ, that is, $\Xi \subset S = \mathbf{v}_0 + S_0$, where $S_0 \subseteq \mathbb{R}^K$ is a subspace and $\mathbf{v}_0 \in \mathbb{R}^K$ is orthogonal to S. Noting that for any $\boldsymbol{\xi} \in \Xi \subset S$, the vectors $(\boldsymbol{\xi} - \mathcal{P}_S(\boldsymbol{\alpha}))$ and $(\mathcal{P}_S(\boldsymbol{\alpha}) - \boldsymbol{\alpha})$ are orthogonal, we have

$$\|\boldsymbol{\xi} - \boldsymbol{\alpha}\|^2 = \|\boldsymbol{\xi} - \mathcal{P}_S(\boldsymbol{\alpha})\|^2 + \|\mathcal{P}_S(\boldsymbol{\alpha}) - \boldsymbol{\alpha}\|^2 . \tag{20}$$

It follows that

$$\begin{aligned} \mathcal{P}_\Xi(\boldsymbol{\alpha}) &\stackrel{\text{def}}{=} \arg\min_{\boldsymbol{\xi}\in\Xi} \|\boldsymbol{\xi} - \boldsymbol{\alpha}\| \\ &= \min_{\boldsymbol{\xi}\in\Xi} \|\boldsymbol{\xi} - \mathcal{P}_S(\boldsymbol{\alpha})\| \stackrel{\text{def}}{=} \mathcal{P}_\Xi\left(\mathcal{P}_S(\boldsymbol{\alpha})\right) \end{aligned} \tag{21}$$

Because Ξ is convex, $\mathcal{P}_\Xi\left(\mathcal{P}_S(\boldsymbol{\alpha})\right)$ can be found by first computing the projection of $\mathcal{P}_S(\boldsymbol{\alpha})$ on each of the facets of the polytope, and then selecting the one with minimum distance to $\mathcal{P}_S(\boldsymbol{\alpha})$ that is,

$$\mathcal{P}_\Xi(\boldsymbol{\alpha}) = \arg \min_{\substack{\mathcal{P}_{\Xi_{f_j}}(\boldsymbol{\alpha}_S) \\ j=1,\ldots,M_\Xi}} \left\| \mathcal{P}_{\Xi_{f_j}}(\mathcal{P}_S(\boldsymbol{\alpha})) - \mathcal{P}_S(\boldsymbol{\alpha}) \right\|, \tag{22}$$

where Ξ_{f_j} is the j^{th} facet of Ξ, and M_Ξ is the total number of facets for Ξ. Since each Ξ_{f_j} is itself a polytope, finding $\mathcal{P}_{\Xi_{f_i}}(\boldsymbol{\alpha}_S)$ follows the same steps just described, with Ξ_{f_i} and $\boldsymbol{\alpha}_S$ taking the place of Ξ and $\boldsymbol{\alpha}$, respectively. Thus, (22) enables recursive computation of the projection of $\boldsymbol{\alpha}$ onto the polytope Ξ, which is summarized in Algorithm 2. With each recursion in Algorithm 2, a projection is computed onto a polytope's face of lower dimensionality until one of the "base cases" are reached, i.e., either the projection on the affine subspace falls inside the polytope, or it is a projection onto a vertex of Ξ.

When we set $\Xi = \Omega(\mathbf{t})$, $\boldsymbol{\alpha}$ is projected onto the MCS. The vertices of $\Omega(\mathbf{t})$, required in Algorithm 2, can be obtained by recalling that the $(K-3)$ dimensional affine subspace $S = \mathbf{v}_0 + S_0 \supseteq \Omega(\mathbf{t})$, where S_0 is the CBS, is the solution set to the constraint $\mathbf{t} = \mathbf{P}\boldsymbol{\alpha}$. For $K = 3$ this implies that $S = \Omega(\mathbf{t})$ is a single point $\boldsymbol{\nu}_1$, the only vertex of the MCS. For $K \geq 4$, the affine subspace is unbounded so the vertices of the MCS lie on the intersection of S with the surface of the hypercube $[0,1]^K$, the feasibility constraint (see , Eqn. (8) in the companion Part I paper [2]). Consequently, the control vector $\boldsymbol{\nu}_i$ corresponding to a vertex of $\Omega(\mathbf{t})$ has all but three of its components as either 0 or 1, and the remaining three components are determined by the colorimetric requirement $\mathbf{t} = \mathbf{P}\boldsymbol{\nu}_i$. With this characterization, the vertices of $\Omega(\mathbf{t})$ can be found via exhaustive search. Vertex candidates $\boldsymbol{\nu} = [\nu_1, \ldots, \nu_K]^T$ are first determined by setting $(K-3)$ components in the vector equal to $0/1$ and determining the remaining components to satisfy the colorimetric constraint. If the candidate is feasible, i.e., has all components between 0 and 1, it is a vertex of the MCS $\Omega(\mathbf{t})$, otherwise it is not. The vertex candidates are readily enumerated by considering each of the $\binom{K}{3}$ selections of three indices between 1 and K, and evaluating the feasibility of the vertex candidates obtained by setting the remaining $(K-3)$ components to every possible 2^{K-3} combination of binary (0/1) values. Thus $\binom{K}{3} \times 2^{K-3}$ vertex candidates are assessed for feasibility. Algorithm 3 summarizes the overall procedure for computation of the vertices of the MCS $\Omega(\mathbf{t})$. Because this procedure is performed only once for a given primary system, the computational (in)efficiency of the process is not of practical concern[6].

APPENDIX C
NUMERICAL COMPUTATION OF THE LAPLACIAN OPERATOR

The Laplacian $\nabla^2 \alpha_k^{\mathscr{F}}(\cdot)$ required for the computation of the variational derivatives in (8) is numerically evaluated over the discrete rectilinear grid $\{\boldsymbol{\tau}_i\}_\epsilon$ used for computing the CCF. Let $\boldsymbol{\tau}$ be a point in the rectangular grid $\{\boldsymbol{\tau}_i\}_\epsilon$. Considering the points in $\{\boldsymbol{\tau}_i\}_\epsilon$ that define the $3\times3\times3$ cubic neighborhood of $\boldsymbol{\tau}$ in (see Fig. 7), the Laplacian for the k^{th} component of the CCF at $\boldsymbol{\tau}$ is approximated as [12]

$$\begin{aligned} \nabla^2 \alpha_k^{\mathscr{F}}(\boldsymbol{\tau}) \approx \frac{3}{13\epsilon^2} \Bigg(& \sum_{\boldsymbol{\tau}_i \in \mathcal{N}_f} \left(\alpha_k^{\mathscr{F}}(\boldsymbol{\tau}_i) - \alpha_k^{\mathscr{F}}(\boldsymbol{\tau})\right) + \\ & \frac{1}{2} \sum_{\boldsymbol{\tau}_i \in \mathcal{N}_e} \left(\alpha_k^{\mathscr{F}}(\boldsymbol{\tau}_i) - \alpha_k^{\mathscr{F}}(\boldsymbol{\tau})\right) + \\ & \frac{1}{3} \sum_{\boldsymbol{\tau}_i \in \mathcal{N}_v} \left(\alpha_k^{\mathscr{F}}(\boldsymbol{\tau}_i) - \alpha_k^{\mathscr{F}}(\boldsymbol{\tau})\right) \Bigg), \end{aligned} \tag{23}$$

where $\mathcal{N}_f$ refers to the set of neighbors lying on center of the facets of the neighborhood cube, $\mathcal{N}_e$ of those lying on the center of the edges, and $\mathcal{N}_v$ refers to the vertices, as described in Fig. 7. The numerical computations of the gradient of the CCFs uses the 19 point stencil approximation for the gradient from [12] that conforms with the chosen Laplacian

[6] As an alternative to the approach presented here, standard quadratic programming [42] can be used to compute the MCS projection. However, we found quadratic programming to be slower than the proposed approach for the typical number of primaries considered here.

Algorithm 2: Projection onto a Polytope

Input : $\boldsymbol{\alpha}$: vector in $\mathbb{R}^K$,
Ξ: Polytope
Output: $\hat{\boldsymbol{\alpha}} = \mathcal{P}_\Xi(\boldsymbol{\alpha})$: projection of $\boldsymbol{\alpha}$ onto Ξ

/* Base Cases: */
$\boldsymbol{\nu}_1, \ldots, \boldsymbol{\nu}_{N_\Xi} \leftarrow$ vertices of Ξ;
// (a): Polytope is single point
if $N_\Xi = 1$ **then**
  $\hat{\boldsymbol{\alpha}} \leftarrow \boldsymbol{\nu}_1$;
  return ;
end
// (b): Project $\boldsymbol{\alpha}$ onto affine subspace $S = \mathbf{v}_0 + S_0 \supset \Xi$
$\mathbf{B} \leftarrow$ Orthonormal Basis for $S_0 = \text{span}\,(\boldsymbol{\nu}_2 - \boldsymbol{\nu}_1, \ldots, \boldsymbol{\nu}_{N_\Xi} - \boldsymbol{\nu}_1)$;
$\mathbf{v}_0 \leftarrow \boldsymbol{\nu}_1 - \mathbf{B}\mathbf{B}^T\boldsymbol{\nu}_1$;
$\boldsymbol{\alpha}_S \leftarrow \mathbf{v}_0 + \mathbf{B}\mathbf{B}^T\boldsymbol{\alpha}$;
if $\boldsymbol{\alpha}_S \in \Xi$ **then**
  $\hat{\boldsymbol{\alpha}} \leftarrow \boldsymbol{\alpha}_S$;
  return;
end
/* Recursion: */
$\Xi_{f_1}, \ldots, \Xi_{f_{M_\Xi}} \leftarrow$ facets of Ξ ;
// Project $\boldsymbol{\alpha}_S$ onto each facet
forall $1 \le j \le M_\Xi$ **do**
  $\boldsymbol{\alpha}_{\Xi_{f_j}} \leftarrow \mathcal{P}_{\Xi_{f_j}}(\boldsymbol{\alpha}_S)$;
end
// Select projection closest to $\boldsymbol{\alpha}_S$
$\hat{\boldsymbol{\alpha}} \leftarrow \arg \min_{\substack{\boldsymbol{\alpha}_{\Xi_{f_j}} \\ 1 \le j \le M_\Xi}} \left(\left\| \boldsymbol{\alpha}_{\Xi_{f_j}} - \boldsymbol{\alpha}_S \right\| \right)$;

approximation. Specifically, the partial derivatives of $\alpha_k^{\mathscr{F}}(\cdot)$ along the direction of τ_j, with $j \in \mathscr{C}$, is computed as,

$$\frac{\partial \alpha_k^{\mathscr{F}}}{\partial \tau_j} \approx \frac{1}{\epsilon h}\Bigg(\sum_{\boldsymbol{\tau}_i \in \mathcal{N}_f} \left(\alpha_k^{\mathscr{F}}(\boldsymbol{\tau}_{i+}) - \alpha_k^{\mathscr{F}}(\boldsymbol{\tau}_{i-})\right) + \frac{1}{\sqrt{2}} \sum_{\boldsymbol{\tau}_i \in \mathcal{N}_e} \left(\alpha_k^{\mathscr{F}}(\boldsymbol{\tau}_{i+}) - \alpha_k^{\mathscr{F}}(\boldsymbol{\tau}_{i-})\right) + \frac{1}{\sqrt{3}} \sum_{\boldsymbol{\tau}_i \in \mathcal{N}_v} \left(\alpha_k^{\mathscr{F}}(\boldsymbol{\tau}_{i+}) - \alpha_k^{\mathscr{F}}(\boldsymbol{\tau}_{i-})\right) \Bigg), \quad (24)$$

where $h = 2 + \frac{8}{\sqrt{2}} + \frac{8}{\sqrt{3}}$, and $\boldsymbol{\tau}_{i+}$ and $\boldsymbol{\tau}_{i-}$ are a pair of opposite neighbors along the directions represented by the line segments in Fig. 8.

Algorithm 3: Computation of Vertices of MCS $\Omega(\mathbf{t})$

Input : $\mathbf{t}$: 3×1 CIE XYZ tristimulus vector for color in gamut $\mathcal{G}$
$\mathbf{P}$: $3 \times K$ matrix of primary CIE XYZ tristimulus vectors
$\mathbf{T}$: $(K-3) \times 2^{K-3}$ array with columns enumerating all $0/1$ assignments to $(K-3)$ variables
$\mathbf{C}$: $3 \times \binom{K}{3}$ array enumerating all selections of three distinct indices from $\{1, \ldots, K\}$
Output: N_Ω: Number of vertices of MCS $\Omega(\mathbf{t})$
$\mathbf{V}_\Omega$: $K \times N_\Omega$ array of vertices of MCS $\Omega(\mathbf{t})$

$N_\Omega \leftarrow 0$; // Initialization
for $n \leftarrow 1$ **to** $\binom{K}{3}$ **do**
  /* Get n^{th} three-primary selection from $\mathbf{P}$ */
  $[i_1, i_2, i_3]^T \leftarrow \mathbf{C}[1:3, n]$;
  $\mathbf{P}_3 \leftarrow [\mathbf{p}_{i_1}, \mathbf{p}_{i_2}, \mathbf{p}_{i_3}]$;
  /* Get remaining $K-3$ primaries from $\mathbf{P}$ */
  $i_4, \ldots, i_K \leftarrow \{1, \ldots, K\} \setminus \{i_1, i_2, i_3\}$;
  $\mathbf{P}_{K-3} \leftarrow [\mathbf{p}_{i_4}, \ldots, \mathbf{p}_{i_K}]$;
  /* Consider all 0/1 primary combinations from $\mathbf{P}_{K-3}$ */
  for $m \leftarrow 1$ **to** 2^{K-3} **do**
    // Compute putative control vector
    $\boldsymbol{\alpha}_{K-3} \leftarrow \mathbf{T}[1:(K-3), m]$;
    $\mathbf{t}_0 \leftarrow \mathbf{P}_{K-3}\boldsymbol{\alpha}_{K-3}$;
    $\boldsymbol{\alpha}_3 \leftarrow \mathbf{P}_3^{-1}(\mathbf{t} - \mathbf{t}_0)$;
    if $\boldsymbol{\alpha}_3 \in [0,1]^3$ **then** // Is Feasible
      // Add to vertex list
      $\nu_{i_1}, \nu_{i_2}, \nu_{i_3} \leftarrow \boldsymbol{\alpha}_3$;
      $\nu_{i_4}, \ldots, \nu_{i_K} \leftarrow \boldsymbol{\alpha}_{K-3}$;
      $\boldsymbol{\nu} \leftarrow [\nu_1, \ldots, \nu_K]^T$;
      $N_\Omega \leftarrow N_\Omega + 1$;
      $\mathbf{V}_\Omega[1:K, N_\Omega] \leftarrow \boldsymbol{\nu}$;
    end
end

REFERENCES

[1] C. E. Rodríguez-Pardo and G. Sharma, "Multiprimary display color calibration: A variational framework for robustness to device variation," in *IS&T Electronic Imaging: Color Imaging XXI: Displaying, Processing, Hardcopy, and Applications*, vol. 2016, no. 20, San Francisco, California, Feb. 2016, pp. COLOR–304.1–7.

[2] C. E. Rodríguez-Pardo and G. Sharma, "Color Control Functions for Multiprimary Displays I: Robustness Analysis and Optimization Formulations," *IEEE Trans. Image Proc.*, vol. 28, 2019, accepted for publication, to appear.

[3] H. J. Trussell, "DSP solutions run the gamut for color systems," *IEEE Sig. Proc. Mag.*, vol. 10, no. 2, pp. 8–23, Apr. 1993.

[4] G. Sharma and H. J. Trussell, "Digital color imaging," *IEEE Trans. Image Proc.*, vol. 6, no. 7, pp. 901–932, Jul. 1997.

[5] M. J. Vrhel and H. J. Trussell, "Color device calibration: A mathematical formulation," *IEEE Trans. Image Proc.*, vol. 8, no. 12, pp. 1796–1806, Dec. 1999.

[6] C. E. Rodríguez-Pardo and G. Sharma, "Calibration sets for multiprimary displays: Representation, visualization, and applications," in *Proc. IS&T/SID 22nd Color and Imaging Conference*, Boston, MA, 3-7 Nov. 2014, pp. 171–179.

[7] I. Gelfand and S. Fomin, *Calculus of variations. Revised English edition translated and edited by Richard A. Silverman*. Englewood Cliffs, NJ: Prentice-Hall Inc., 1963.

[8] A. A. Goldstein, "Convex programming in Hilbert space," *Bull. Amer. Math. Soc.*, vol. 70, no. 5, pp. 709–710, 1964.

[9] P. H. Calamai and J. J. Moré, "Projected gradient methods for linearly constrained problems," *Math. Program.*, vol. 39, no. 1, pp. 93–116, 1987.

[10] D. Bertsekas, "On the Goldstein-Levitin-Polyak gradient projection method," *IEEE Trans. Automatic Control*, vol. 21, no. 2, pp. 174–184, 1976.

[11] G. Sharma, "Color fundamentals for digital imaging," in *Digital Color Imaging Handbook*, G. Sharma, Ed. Boca Raton, FL: CRC Press, 2003, chapter 1.

[12] R. C. O'Reilly and J. M. Beck, "A family of large-stencil discrete

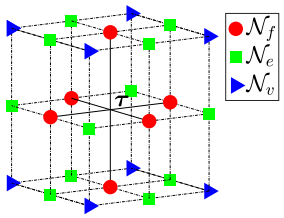

Fig. 7: The $3 \times 3 \times 3$ cubic neighborhood of the point $\boldsymbol{\tau}$ in the uniform grid $\{\boldsymbol{\tau}_i\}_\epsilon$ used for numerical computation of the Laplacian using the 27 point stencil approximation [12]. The node for color $\boldsymbol{\tau}$ lies at the center and its 26 neighbors are can be grouped into subsets $\mathcal{N}_f$, $\mathcal{N}_e$, and $\mathcal{N}_v$, corresponding respectively, to the nodes located at the facet centers, midpoints of edges, and vertices of the neighborhood cube, as shown.

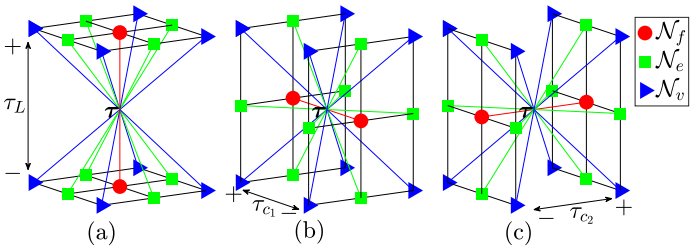

Fig. 8: The $3 \times 3 \times 3$ cubic neighborhood of the point $\boldsymbol{\tau}$ in the uniform grid $\{\boldsymbol{\tau}_i\}_\epsilon$ used for numerical computation of the gradient using the 19 point stencil approximation [12]. The node for color $\boldsymbol{\tau}$ lies at the center and the computation of the gradient involves 18 of its neighbors, grouped into subsets $\mathcal{N}_f$, $\mathcal{N}_e$, and $\mathcal{N}_v$. Figures (a), (b) and (c) show how the differences between neighbors are computed for the gradient along τ_L, τ_{c_1}, and τ_{c_2}, respectively.

Laplacian approximations in three dimensions," *Int. J. Numer. Meth. Eng.*, pp. 1–16, 2006.

[13] P. Centore, "Non-metamerism of boundary colors in multi-primary displays," *J. Soc. Inf. Display*, vol. 20, no. 4, pp. 214–220, 2012.

[14] S. Wen, "Design of relative primary luminances for four-primary displays," *Displays*, vol. 26, no. 4-5, pp. 171 – 176, 2005.

[15] H. Xie, C. E. Rodríguez-Pardo, and G. Sharma, "Multi-objective optimization for color display primary designs," *J. Electronic Imaging*, vol. 26, no. 6, p. 063013, 2017.

[16] C. E. Rodríguez-Pardo, G. Sharma, and X.-F. Feng, "Primary selection for uniform display response," in *Proc. SPIE: Color Imaging XIX: Displaying, Processing, Hardcopy, and Applications*, vol. 9015, Feb. 2014, pp. 90 150I–1–90 150I–9.

[17] D. L. MacAdam, "Maximum visual efficiency of colored materials," *J. Opt. Soc. Am.*, vol. 25, no. 11, pp. 361–367, 1935.

[18] F. Konig, K. Ohsawa, M. Yamaguchia, N. Ohyama, and B. Hill, "A multiprimary display: Optimized control values for displaying tristimulus values," in *Proc. IS&T/SID PICS 2002: Image Processing, Image Quality, Image Capture Systems Conference*. Society for Imaging Science & Technology, 2002, pp. 215–220.

[19] M. Takaya, K. Ito, G. Ohashi, and Y. Shimodaira, "Color-conversion method for a multi-primary display to reduce power consumption and conversion time," *J. Soc. Inf. Display*, vol. 13, no. 8, pp. 685–690, 2012.

[20] P. Centore, "Minimal-energy control sequences for linear multi-primary displays," *J. Imaging Sci. and Tech.*, vol. 59, no. 5, pp. 50 502–1–10, 2015.

[21] IEC, "Colour measurement and management in multimedia systems and equipment, part 2-1: Colour management - default RGB colour space-sRGB," IEC Publication No. 61966-2.1, 1999.

[22] CIE, "Colorimetry," CIE Publication No. 15:2004, Central Bureau of the CIE, Vienna, 2004.

[23] G. J. Braun, M. D. Fairchild, and F. Ebner, "Color gamut mapping in a hue-linearized CIELAB color space," in *Proc. IS&T/SID Sixth Color Imaging Conference: Color Science, Systems and Applications*, Scottsdale, AZ, 17-20 Nov. 1998, pp. 163–168.

[24] K. McLaren, "CIELAB hue-angle anomalies at low tristimulus ratios," *Color Res. Appl.*, vol. 5, no. 3, pp. 139–143, 1980.

[25] G. Sharma and C. E. Rodríguez-Pardo, "The dark side of CIELAB," in *Proc. SPIE: Color Imaging XVII: Displaying, Hardcopy, Processing, and Applications*, vol. 8292, Jan. 2012, pp. 8292–0D,1–10.

[26] C. Li, Z. Li, Z. Wang, Y. Xu, M. R. Luo, G. Cui, M. Melgosa, M. H. Brill, and M. Pointer, "Comprehensive color solutions: CAM16, CAT16, and CAM16-UCS," *Color Res. Appl.*, vol. 42, no. 6, pp. 703–718, 2017.

[27] CIE, "Improvement to industrial colour-difference evaluation," CIE Publication No. 142-2001, Central Bureau of the CIE, Vienna, 2001.

[28] G. Sharma, W. Wu, and E. N. Dalal, "The CIEDE2000 color-difference formula: Implementation notes, supplementary test data, and mathematical observations," *Color Res. Appl.*, vol. 30, no. 1, pp. 21–30, Feb. 2005.

[29] J.-M. Morel and S. Solimini, *Variational methods in image segmentation*. Boston: Birkhäuser, 1995.

[30] J. Weickert, *Anisotropic diffusion in image processing*. Teubner Stuttgart, 1998.

[31] O. Scherzer, M. Grasmair, H. Grossauer, M. Haltmeier, and F. Lenzen, *Variational methods in imaging*. New York: Springer, 2009.

[32] R. Kimmel, D. Shaked, M. Elad, and I. Sobel, "Space-dependent color gamut mapping: A variational approach," *IEEE Trans. Image Proc.*, vol. 14, no. 6, pp. 796–803, 2005.

[33] International Color Consortium, "Visualization of medical content on color display systems," White Paper # 44, Apr. 2016. [Online]. Available: http://www.color.org/whitepapers/ICC_White_Paper44_Visualization_of_colour_on_medical_displays.pdf

[34] T. Ajito, K. Ohsawa, T. Obi, M. Yamaguchi, and N. Ohyama, "Color conversion method for multiprimary display using matrix switching," *Opt. Rev.*, vol. 8, no. 2, pp. 191–197, 2001.

[35] D.-W. Kang, Y.-H. Cho, Y.-T. Kim, W.-H. Choe, and Y.-H. Ha, "Multiprimary decomposition method based on a three-dimensional look-up table in linearized LAB space for reproduction of smooth tonal change," *J. Imaging Sci. and Tech.*, vol. 50, no. 4, pp. 357–367, 2006.

[36] H. Kanazawa, M. Mitsui, M. Yamaguchi, H. Haneishi, and N. Ohyama, "Color conversion for multi-primary displays using a spherical average method," in *Proc. IS&T/SID Twelfth Color Imaging Conference: Color Science and Engineering: Systems, Technologies, Applications*, Scottsdale, AZ, 9-12 Nov. 2004, pp. 65–69.

[37] P. Centore and M. H. Brill, "Extensible multi-primary control sequences," *J. Soc. Inf. Display*, vol. 20, no. 1, pp. 12–21, 2012.

[38] H. Motomura, "Color conversion for a multi-primary display using linear interpolation on equi-luminance plane method (LIQUID)," *J. Soc. Inf. Display*, vol. 11, no. 2, pp. 371–378, 2003.

[39] Y. Murakami, N. Hatano, J. Takiue, M. Yamaguchi, and N. Ohyama, "Evaluation of smooth tonal change reproduction on multiprimary display: comparison of color conversion algorithms," in *Proc. SPIE: Color Imaging X: Processing, Hardcopy, and Applications*, vol. 5289, Jan. 2004, pp. 275–283.

[40] H. W. Ok, S. D. Lee, W. H. Choe, D. S. Park, and C. Y. Kim, "Color processing for multi-primary display devices," in *Proc. IEEE Intl. Conf. Image Proc.*, vol. 3, Sept. 2005, pp. III–980.

[41] M. Giaquinta and S. Hildebrandt, *Calculus of variations I*. Berlin: Springer-Verlag, 2004.

[42] D. G. Luenberger and Y. Ye, *Linear and nonlinear programming*. Berlin: Springer, 2008.

Carlos Eduardo Rodríguez-Pardo , for a biography, see this issue, p. TBD.

Gaurav Sharma (S'88–M'96–SM'00–F'13), for a biography, see this issue, p. TBD.